Assessing crosstalk in simultaneous multicolor single-molecule localization microscopy

Karoline Friedl, Adrien Mau, Fanny Boroni-Rueda, Valentina Caorsi, Nicolas Bourg, Sandrine Lévêque-Fort, Christophe Leterrier

Cell Reports
Methods

Article

Assessing crosstalk in simultaneous multicolor single-molecule localization microscopy

Graphical abstract

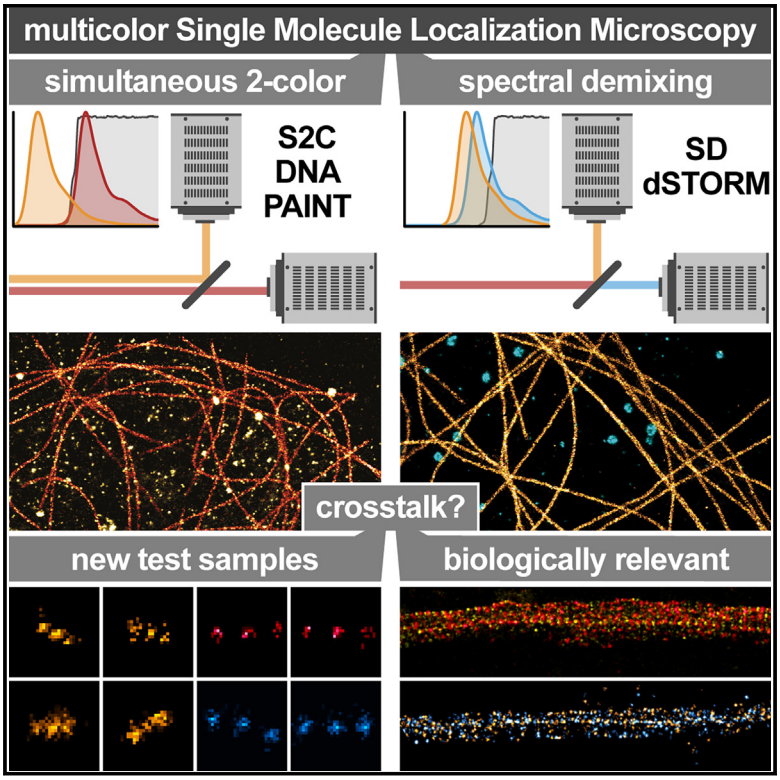

Highlights

- Multicolor single-molecule localization microscopy (SMLM) is slow and difficult
- We use a two-camera module to compare spectral separation and demixing approaches
- We propose new samples and procedures to assess crosstalk in multicolor SMLM
- Spectral demixing is a robust approach for two- to three-color SMLM in 2D and 3D

Authors

Karoline Friedl, Adrien Mau, Fanny Boroni-Rueda, Valentina Caorsi, Nicolas Bourg, Sandrine Lévêque-Fort, Christophe Leterrier

Correspondence

christophe.leterrier@univ-amu.fr

In brief

Friedl et al. use a two-camera module to assess the performance of two simultaneous multicolor single-molecule localization microscopy approaches. Focusing on the rigorous assessment of crosstalk between channels, they conclude that spectral demixing of several far-red fluorophores is a fast and robust approach for two- to three-color nanoscopy.

Friedl et al., 2023, Cell Reports Methods *3*, 100571
September 25, 2023
https://doi.org/10.1016/j.crmeth.2023.100571

CellPress

Please cite this article in press as: Friedl et al., Assessing crosstalk in simultaneous multicolor single-molecule localization microscopy, Cell Reports Methods (2023), https://doi.org/10.1016/j.crmeth.2023.100571

Cell Reports Methods

CellPress
OPEN ACCESS

Article

Assessing crosstalk in simultaneous multicolor single-molecule localization microscopy

Karoline Friedl,[1,2] Adrien Mau,[2,3] Fanny Boroni-Rueda,[1] Valentina Caorsi,[2] Nicolas Bourg,[2] Sandrine Lévêque-Fort,[3] and Christophe Leterrier[1,4,*]

[1]Aix Marseille Université, CNRS, INP UMR7051, NeuroCyto, 13005 Marseille, France
[2]Abbelight, 191 Avenue Aristide Briand, 94230 Cachan, France
[3]Université Paris Saclay, CNRS, Institut des Sciences Moléculaires d'Orsay, 91405 Orsay, France
[4]Lead contact
*Correspondence: christophe.leterrier@univ-amu.fr
https://doi.org/10.1016/j.crmeth.2023.100571

MOTIVATION Single-molecule localization microscopy (SMLM) is a straightforward approach to bypass the diffraction limit of optical microscopy and resolve the arrangement of cellular components in their native environment thanks to its <50 nm resolution. However, SMLM acquisitions are slow, particularly for multicolor experiments where channels are usually acquired in sequence. Here we take advantage of a two-camera module to evaluate the performance of simultaneous two-color SMLM approaches based on spectrally distinct fluorophores or spectral demixing, focusing on the rigorous assessment of the crosstalk between channels.

SUMMARY

Single-molecule localization microscopy (SMLM) can reach sub-50 nm resolution using techniques such as stochastic optical reconstruction microscopy (STORM) or DNA-point accumulation for imaging in nanoscale topography (PAINT). Here we implement two approaches for faster multicolor SMLM by splitting the emitted fluorescence toward two cameras: simultaneous two-color DNA-PAINT (S2C-DNA-PAINT) that images spectrally separated red and far-red imager strands on each camera, and spectral demixing dSTORM (SD-dSTORM) where spectrally close far-red fluorophores appear on both cameras before being identified by demixing. Using S2C-DNA-PAINT as a reference for low crosstalk, we evaluate SD-dSTORM crosstalk using three types of samples: DNA origami nanorulers of different sizes, single-target labeled cells, or cells labeled for multiple targets. We then assess if crosstalk can affect the detection of biologically relevant subdiffraction patterns. Extending these approaches to three-dimensional acquisition and SD-dSTORM to three-color imaging, we show that spectral demixing is an attractive option for robust and versatile multicolor SMLM investigations.

INTRODUCTION

The advent of super-resolution microscopy has allowed bypassing of the diffraction barrier in fluorescence imaging and study of the fine details of the cellular architecture.[1,2] Among the various techniques available to biologists, single-molecule localization microscopy (SMLM) requires relatively simple equipment and can reach a lateral resolution below 50 nm.[3–5] Its principle is to temporally decompose a fluorescent staining into sparsely blinking fluorophores, allowing their localization through single molecule detection and fitting along the successive frames of a continuous acquisition, the final image being generated by plotting all fitted coordinates of the detected fluorophores (also called localizations).[6] One of the first SMLM modalities was based on inducing the sparse blinking of organic fluorophores by high-power laser illumination in a reducing buffer, an approach called (direct) stochastic optical reconstruction microscopy (d)STORM.[7,8] In the more recent DNA-point accumulation for imaging in nanoscale topography (DNA-PAINT) approach, blinking is generated from the transient interaction of short fluorescent DNA strands with their cognate docking strand conjugated to antibodies.[9]

The single molecule nature of SMLM provides its exquisite resolution, but comes with two consequences: it is an inherently slow technique, where fluorophores must be localized one by one; and multicolor labeling is constrained, particularly in dSTORM where buffer-fluorophore combinations must be carefully selected. Sequential imaging of labels slows down the imaging process further, while increasing sample drift during acquisition. Simultaneous multicolor SMLM can be performed using

Please cite this article in press as: Friedl et al., Assessing crosstalk in simultaneous multicolor single-molecule localization microscopy, Cell Reports Methods (2023), https://doi.org/10.1016/j.crmeth.2023.100571

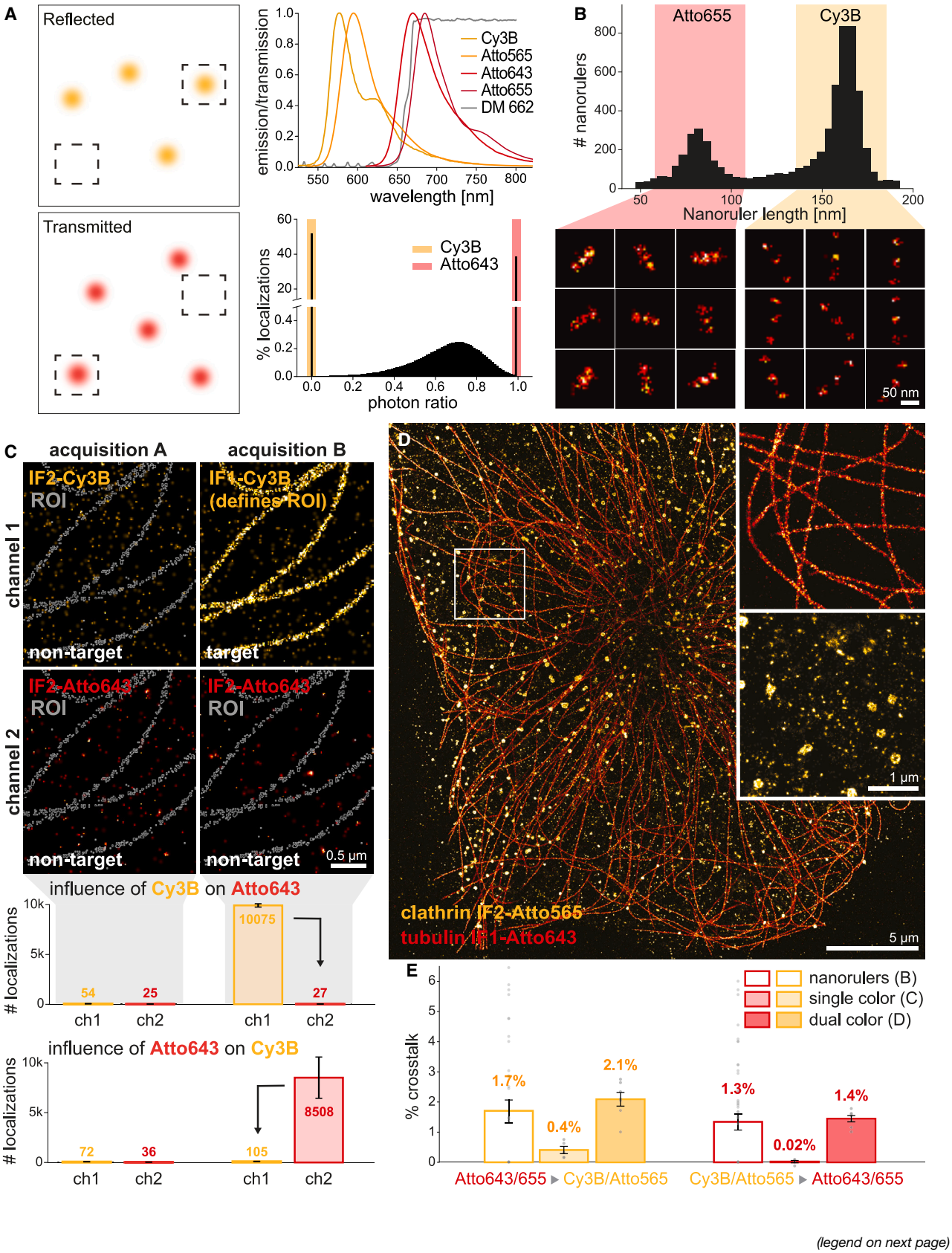

(legend on next page)

Please cite this article in press as: Friedl et al., Assessing crosstalk in simultaneous multicolor single-molecule localization microscopy, Cell Reports Methods (2023), https://doi.org/10.1016/j.crmeth.2023.100571

CellPress
OPEN ACCESS

spectral separation and two-way detection, but is difficult to implement in dSTORM: differences in dye photophysics make it difficult to find a combination providing optimal blinking in the same imaging buffer. DNA-PAINT is more straightforward than dSTORM for multicolor imaging, as it is possible to devise orthogonal DNA sequences and image them successively—a method called exchange-PAINT.[9–11] However, this results in extremely long acquisition times, blinking in DNA-PAINT being inherently slower than dSTORM despite efforts to speed up the transient binding of imager strands.[12–14] A couple of recent attempts have been made to alleviate this through simultaneous two-color PAINT acquisitions.[15,16] Here, a common caveat of simultaneous two-color SMLM is the significant chromatic aberration between the spectrally distinct channels that must be compensated.[17–19]

Another elegant approach for multicolor SMLM is to take advantage of the isolated nature of single molecule blinking events and determine their identity by splitting the emitted fluorescence in two paths using a dichroic mirror, identifying fluorophores based on the balance of intensities detected on each side. This "spectral demixing" strategy was developed soon after SMLM invention, using spectrally close fluorophores illuminated by a single laser.[20–25] The optimal dSTORM combination converged toward using far-red fluorophores such as DY634, Alexa Fluor 647 (AF647), CF647, DL650, CF660C, or CF680.[26–36] Spectral demixing was also recently demonstrated for simultaneous DNA-PAINT with up to three channels.[34] Spectral demixing SMLM images all fluorophores simultaneously, speeding up the acquisition at the cost of a higher blinking density, limiting the processing algorithm capacity to pair blinking events and reliably assigning them to each channel.[32,35,36] In addition, chromatic aberration between spectrally close channels is minimal, and can be easily corrected, as blinking events are visible on both detection pathways.

In multicolor microscopy, it is important to avoid crosstalk between channels—the presence of the signal from one target in the channel where another target is imaged. This is caused by the fluorophores and optical components used (overlapping excitation or emission spectra, insufficient filtering). In multicolor SMLM, non-specific labeling and spurious detection can also be significant sources of crosstalk. When using a spectral demixing strategy, the need to assign spectrally close fluorophores to the different channels may add yet another source of crosstalk. So far, studies using spectral demixing have used theoretical calculations and single-color calibration experiments to address this concern[20,24,33,34]: a more detailed assessment of crosstalk in spectral demixing SMLM would help strengthening the appeal of this approach. We recently developed an SMLM module that couples large field-of-view illumination to a two-way detection path.[37] Here, we used this module to implement and compare two approaches for simultaneous two-color SMLM: spectral separation (simultaneous two-color DNA-PAINT, S2C-DNA-PAINT) as a reference modality with minimal crosstalk, and spectral demixing of two far-red fluorophores excited by a single laser (spectral demixing dSTORM, SD-dSTORM). We developed innovative samples and procedures to assess the crosstalk between channels in both modalities, and evaluate its influence on biologically relevant imaging of neuronal scaffolds. Finally, we demonstrate that both simultaneous S2C-DNA-PAINT and SD-dSTORM are readily extensible to astigmatism-based 3D SMLM, and that SD-dSTORM extension to three colors is straightforward.

RESULTS

Simultaneous two-color DNA-PAINT imaging

Our first strategy for simultaneous multicolor super-resolution imaging is based on the traditional principle of spectral separation in fluorescence microscopy, using a pair of fluorophores with distinct excitation and emission spectra: Cy3B or Atto565 (emitting in the red part of the spectrum) and Atto643 or Atto655 (emitting in the far-red) are continuously excited by 532- and 640-nm lasers, with their emission split by a 662-nm dichroic toward two cameras (Figure S1A). A dSTORM-based implementation of this two-color imaging approach does not provide high-quality images, due to the lower blinking quality of red fluorophores[28,38] (Figure S2). By contrast, DNA-PAINT is a good candidate for two-color imaging by spectral separation, as blinking from the red and far-red strands hybridization occurs

Figure 1. Simultaneous two-color DNA-PAINT (S2C-DNA-PAINT) and crosstalk evaluation

(A) In S2C-DNA-PAINT, blinking events appear only on either one camera or the other (left panels): fluorophores emitting in the red (here Cy3B, orange curve on top right spectra graph) and far-red (here Atto643, red curve) are separated by the 662-nm cutoff dichroic mirror (gray line). Ratiometric analysis (bottom right graph) shows fluorophores appearing on only one camera, leading to the chosen ratio ranges (orange and red colored areas): 0.00–0.01 for Cy3B and 0.99–1.0 for Atto643, used in (B), (C), and (D).

(B) Crosstalk measurement from nanorulers (40-nm and 80-nm spacing) bearing P1 and P3 docking strands using I1-Atto655 and I3-Cy3B imager strands. Nanorulers were classified by total length (top distributions, peaks at 80 and 160 nm) before determining the crosstalk (see Figure S2D).

(C) Crosstalk measurement from a single-target cellular sample: zoomed image of a COS-7 cell labeled for microtubules with a secondary antibody carrying an F1 docking strand. Acquisition A (top, left column) uses a mixture of non-target (IF2) imager strands to measure the background signal in both channels (see Figure S3). Acquisition B (top, right column) is done over the same field of view with a mixture of a target (IF1-Cy3B) and a non-target (IF2-Atto643) imager strands. An ROI enclosing the microtubule network (bottom row, white is an ROI overlay on the background images) is obtained from the target (IF1-Cy3B) image and used to measure the number of localizations for acquisitions A and B in both channels (middle graph). The crosstalk from Cy3B into Atto643 is based on the difference between the number of localizations in acquisition B, channel 2 (right red bar) and the number of localizations in acquisition A, ch2 (left red bar). Conversely, the crosstalk of Atto643 into Cy3B can be measured using a target IF2-Cy3B acquisition, evaluating the difference induced in ch1 between acquisition A and B (orange bars in bottom graph).

(D) Crosstalk measurement from a two-target cellular sample: COS-7 cells labeled for tubulin (F1 docking strand) and clathrin (F2 docking strand), simultaneously imaged with IF1-Atto643 and IF2-Atto565. Insets show zoomed isolated channels. Crosstalk was calculated from exclusive ROIs containing only microtubules or only clathrin-coated pits excluding overlapping areas.

(E) Crosstalk values obtained from the three different approaches, grouped by crosstalk direction (far-red into red on the left, orange; red into far-red on the right, red): nanorulers (B), single-target cellular sample (C), and two-target cellular sample (D). Points correspond to individual images or datapoints, error bars are SEM.

Please cite this article in press as: Friedl et al., Assessing crosstalk in simultaneous multicolor single-molecule localization microscopy, Cell Reports Methods (2023), https://doi.org/10.1016/j.crmeth.2023.100571

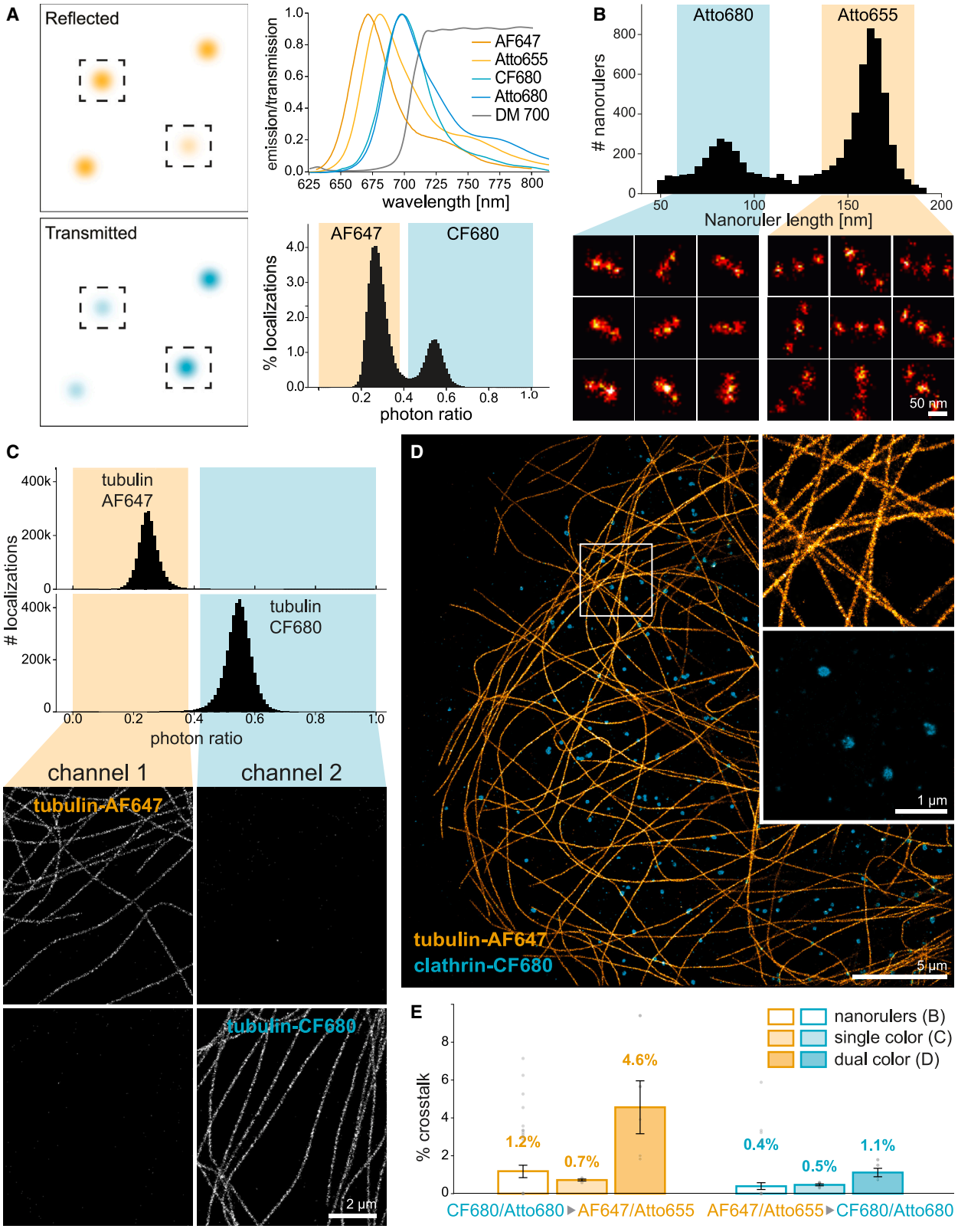

(legend on next page)

Please cite this article in press as: Friedl et al., Assessing crosstalk in simultaneous multicolor single-molecule localization microscopy, Cell Reports Methods (2023), https://doi.org/10.1016/j.crmeth.2023.100571

with similar properties, and the blinking density can be independently adjusted by modifying each imager strand concentration.[9,39] Most multicolor DNA-PAINT studies have used sequential acquisition of targets with different imagers conjugated to the same fluorophore. However, it is straightforward to increase the acquisition speed by simultaneously acquiring two channels using spectrally separated fluorophore on distinct imagers, as demonstrated recently.[15,16]

We thus performed simultaneous two-color acquisition by DNA-PAINT (S2C-DNA-PAINT) using imager strands conjugated with fluorophores emitting in the red channel (Cy3B or Atto565) and far-red channel (Atto643 or Atto655), similar to Chung et al.[16] (Figure 1A). To check if crosstalk can occur for this two-color approach and compare it with the spectral demixing strategy, we performed a ratiometric analysis[22,24]: blinking events were processed, resulting in localization coordinates. Localizations appearing at the same time and within 500 nm of each other on both camera frames were paired, and their ratio of photons calculated by dividing the number of photons in the transmitted pathway T (far-red channel) by the total number of photons found on both cameras $R + T$ (R: red channel). When present only on the reflected pathway frame (red channel), a localization was assigned a ratio of 0, whereas if it was found only on the transmitted pathway frame, it was assigned a ratio of 1. The average photon ratio distribution from S2C-DNA-PAINT acquisitions with the Cy3B/Atto643 imager pair (microtubules and clathrin in COS-7 cells, Figure 1D) is shown in Figure 1A. Only ~3% of the total localizations are paired, showing that most blinking events only appear on one camera. Accordingly, we assigned localizations with ratios between 0 and 0.01 to the red channel, and between 0.99 and 1 for the far-red channel (Figure 1A).

Measurement of crosstalk on three different types of samples

We then used several types of samples to detect the baseline crosstalk of the S2C-DNA-PAINT approach: a mix of DNA origami nanorulers of different sizes[40,41](Figure 1B), cellular samples stained against a single target (tubulin in COS-7 cells, Figure 1C), or against two targets (clathrin and tubulin in COS-7 cells, Figure 1D).[42] The custom nanoruler slide combines two types of three-spot rulers: 80-nm long nanorulers with a 40-nm distance between spots labeled with a P1 docking strand (“short” nanoruler), and 160-nm-long nanorulers with an 80-nm distance between spots labeled with a P3 docking strand (“long” nanoruler). The nanorulers were imaged simultaneously using I1-Atto655 (short) and I3-Cy3B (long) fluorescent imager strands (Figure 1B). We devised these nanorulers to obtain structures identified solely from their shape without relying on channel information, providing an independent way of measuring crosstalk. Approximately 20 nanorulers with clearly resolved structure were chosen from each channel in each of three acquisitions, and we then calculated the crosstalk between channels by measuring the number of localizations found in the non-labeled channel divided by the number of localizations in both the labeled and non-labeled channels (Figure S2D). This nanoruler-based approach led to 1.7% crosstalk from the Atto655 channel into the Cy3B channel, whereas the crosstalk from Cy3B channel into the Atto655 channel was found to be 1.3% (Figure 1E).

A more classic way of assessing crosstalk is to use single-target labeling in cells, and to measure the signal induced in the non-target channel by the labeling in the target channel. This is, however, not applicable when using high-performance SMLM algorithms that detect blinking events based on a relative threshold, as the detection threshold will be lowered in the non-target channel, resulting in the detection of spurious localization events and an overestimated crosstalk. This is especially true when using DNA-PAINT, as the local variation of the fluorescent imager background will provide fitting candidates to an adaptive algorithm in the absence of true blinking events. To assess crosstalk from single-target samples using the same algorithm as for other samples, we devised a method based on repeated imaging of the same field of view, a unique possibility offered by DNA-PAINT. We thus measured the change in localization numbers for a non-target (“empty”) channel that is induced by having an imager strand present in the “target” channel: for example, we observed if more localizations would be detected in the “empty” red channel (devoid of imager), whether an Atto643 imager strand was present and interacted with its cognate docking strand on a cellular labeling in the far-red channel. We prepared COS-7 cells stained for microtubules with an anti-tubulin antibody and a secondary antibody conjugated to an F1 docking sequence, then acquired two sequences. The first sequence used a mixture of IF2-Cy3B and IF2-Atto643 imager strands that both do not bind to the tubulin staining, measuring the number of localizations from the DNA-PAINT background in both channels (Figure 1C, “acquisition A”). To estimate the crosstalk from the Cy3B channel into the Atto643 channel, we then acquired a second sequence on the same field of view,

Figure 2. Spectral demixing STORM (SD-dSTORM) and crosstalk evaluation

(A) In SD-dSTORM, blinking events from two far-red fluorophores (AF647 and CF680) appear on both cameras (left panels) due to their spectral proximity (top right graph). Ratiometric analysis of photon ratios for blinking events from each fluorophore leads to a 0.01–0.38 range for AF647 (yellow area), and 0.42–0.99 for CF680 (blue area), used in (B), (C), and (D).

(B) Crosstalk measurement from nanorulers (40-nm and 80-nm spacing) bearing P1 and P3 docking strands and imaged with I1-Atto680 and I3-655 imager strands. Nanorulers were classified by total length (top distribution, peaks 80 and 160 nm) before determining the crosstalk.

(C) Crosstalk measurement from a single-target cellular sample: COS-7 cells labeled for microtubules with a secondary antibody conjugated to either AF647 or CF680 with ratiometric analysis of the localizations (top). After demixing (yellow and blue areas), images were reconstructed (bottom panels). ROIs were drawn around the microtubules with an intensity threshold and used on both channels to calculate the crosstalk.

(D) Crosstalk measurement from a two-target cellular sample: COS cells labeled for tubulin with AF647 and for clathrin with CF680. Insets show zoomed isolated channels. Crosstalk was calculated from exclusive ROIs containing only microtubules or only clathrin-coated pits excluding overlapping areas.

(E) Crosstalk values obtained from the three different approaches, grouped by crosstalk direction (far-red into red on the left, orange; red into far-red on the right, red): nanorulers (see B), single-target cellular sample (C), and two-target cellular sample (D). Points correspond to individual images or datapoints, error bars are SEM.

Please cite this article in press as: Friedl et al., Assessing crosstalk in simultaneous multicolor single-molecule localization microscopy, Cell Reports Methods (2023), https://doi.org/10.1016/j.crmeth.2023.100571

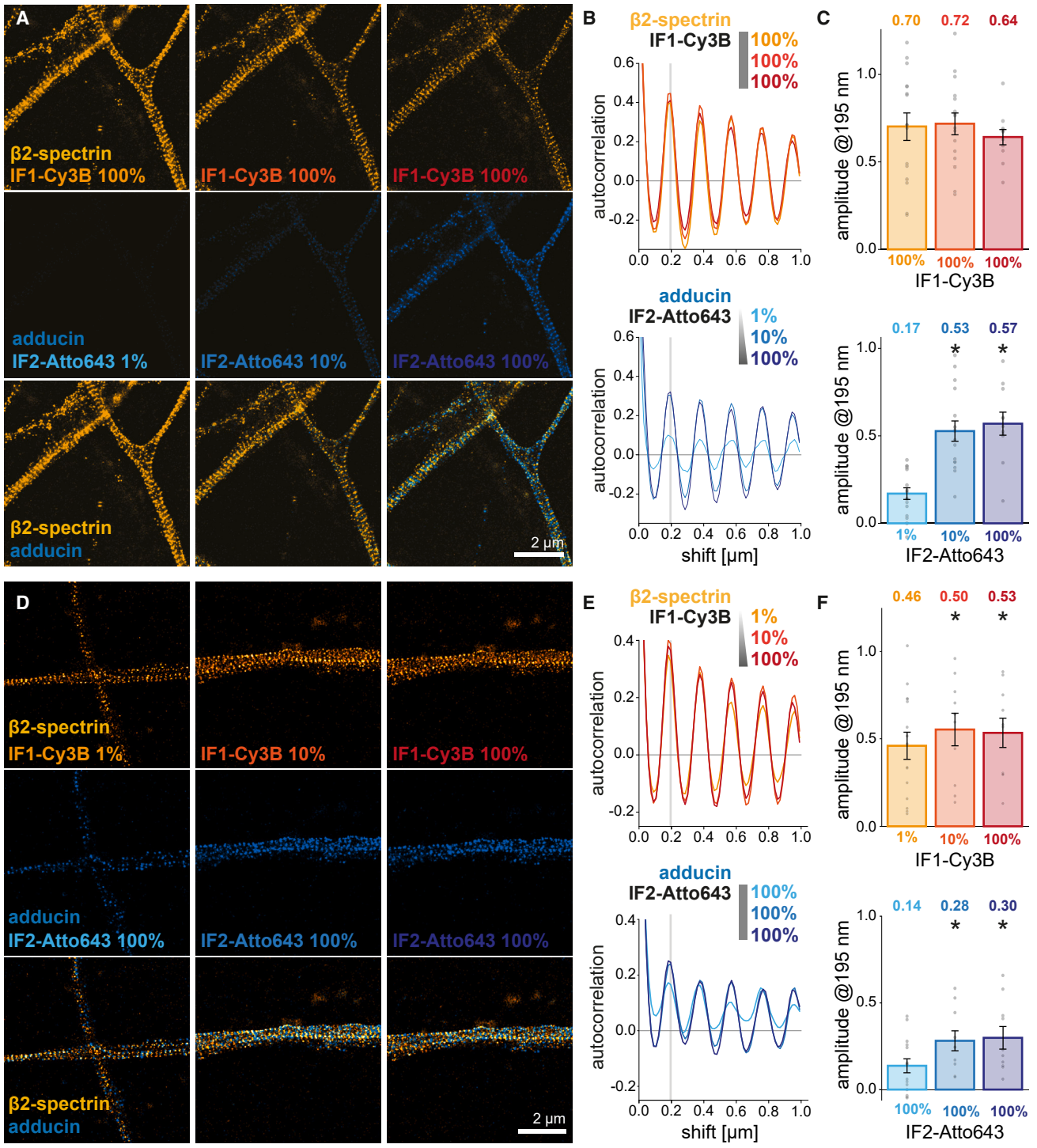

Figure 3. Effect of crosstalk on the detection of biologically relevant patterns by S2C-DNA-PAINT

(A) Reconstructed images of axons stained for β2-spectrin (orange) and adducin (blue), imaged by S2C-DNA-PAINT using IF1-Cy3B and IF2-Atto643, respectively. On the same field of view, the imager concentration of IF1-Cy3B (β2-spectrin) was kept constant, while the concentration of IF2-Atto643 (adducin) was increased successively from 1% to 10% and 100% of the reference concentration.

(B) Autocorrelation curves from 1-µm-long intensity profiles along axons for the constant β2-spectrin-IF1-Cy3B (orange) and varying adducin-IF2-Atto643 (blue) channels for each imager concentration conditions.

(C) Amplitude of the autocorrelation first peak for each imager concentration value.

(legend continued on next page)

Please cite this article in press as: Friedl et al., Assessing crosstalk in simultaneous multicolor single-molecule localization microscopy, Cell Reports Methods (2023), https://doi.org/10.1016/j.crmeth.2023.100571

this time with a mixture of the IF1-Cy3B and IF2-Atto643 imager strands (Figure 1C, "acquisition B"). In this second acquisition sequence, the microtubule staining is revealed in the Cy3B channel, whereas the Atto643 channel contains background plus the crosstalk from the Cy3B channel staining. We segmented the microtubule staining in the Cy3B channel (Figure 1C, upper right panel), and used the resulting region of interest (ROI) to measure the number of localizations in the Atto643 channel from each of the two acquired sequences (Figure 1C, white outlines). The crosstalk was calculated as the difference in the number of localizations within this ROI in the Atto643 channel when the Cy3 channel contains a target (acquisition B) and non-target (acquisition A) imager strand, divided by the background-corrected number of localizations in both channels (see Figure S3 and STAR Methods). Conversely, we acquired another pair of sequences to measure the crosstalk from the Atto643 channel into the Cy3B channel on F1-labeled microtubules. For this, the same acquisition A was performed with IF2-Cy3B and IF2-Atto643 imager strands, while acquisition B was performed with the IF2-Cy3B and IF1-Atto643 imager strands (Figure 1C). With this approach, we found very low values of crosstalk with S2C-DNA-PAINT: the Atto643 channel crosstalk into Cy3B was 0.41%, while the Cy3B channel crosstalk into the Atto643 channel was 0.02% (Figure 1E).

Finally, we aimed at directly measuring the crosstalk from simultaneously acquired two-color DNA-PAINT images. We prepared COS-7 cells labeled for clathrin-coated pits (anti-clathrin primary antibody with secondary antibody conjugated with an F2 docking sequence) and for microtubules (anti-tubulin primary antibody with secondary antibody conjugated with an F1 docking strand). The sample was imaged with a mixture of IF2-Atto565 and IF1-Atto643, and the two channels were obtained after demixing as detailed above (ratio range 0.0–0.01 for the Atto565 channel, 0.99–1.0 for the Atto643 channel) followed by channel registration to compensate for chromatic aberration and camera misalignment (Figure S5). The reconstructed images show no visible crosstalk between channels (Figure 1D) and a good structural quality for both targets, similar to what we can obtain with each acquired DNA-PAINT channel in alternating frames.[42] To measure the crosstalk from these data, we generated ROIs that contained localizations from a single target, excluding regions where pits and microtubules overlap: the microtubule network and the clathrin-coated pits were segmented, then exclusive-target ROIs were derived by excluding overlapping areas using ROI subtraction (Figure S4). We calculated the crosstalk in each exclusive-target ROI as the number of localizations within the exclusive-target ROI on the non-target image (example: microtubule-only ROI applied on the clathrin-coated pits image), divided by the sum of the localizations on the target and non-target images within the same ROI (example: sum of the localizations from the microtubules and clathrin-coated pits images within the microtubule-only ROI). We obtained a crosstalk value of 2.1% for the Atto643 channel crosstalk into the Cy3B channel, and of 1.4% for Cy3B into Atto643 (Figure 1E).

A comprehensive overview of all acquisition parameters can be found in Table S1. Overall, we found higher crosstalk values from the two-target samples and nanorulers compared with the background-corrected single-target samples. This is likely due to the specific procedure used with single-target samples that eliminates background from non-specific imager binding and spurious detections of the fluctuating imager background. Thus, in S2C-DNA-PAINT, these are the main source of the ~1%–2% observed crosstalk, as optical crosstalk from spectral overlap is expected to be minimal. The three methods were consistent in detecting more crosstalk from the higher-wavelength channel (far-red Atto643/Atto655) into the lower-wavelength channel (red Cy3B/Atto565), which is likely to correspond to more spurious detections in the latter.

Simultaneous two-channel imaging using spectral demixing of two far-red fluorophores

We next implemented spectral demixing of two far-red fluorophores to assess how this approach compares with spectrally separated two-color imaging in terms of crosstalk. Fluorophores were excited by a single laser illumination at 640 nm, their emission was split using a 700-nm long-pass dichroic mirror into a reflected and transmitted pathway, and blinking events from both fluorophores appeared on each camera (Figures 2A and S1B). A ratiometric analysis was performed as for S2C-DNA-PAINT imaging: the average photon ratio distribution from several spectral demixing acquisitions (microtubules and clathrin in COS-7 cells, Figure 2D) using AF647 and CF680 fluorophores showed a photon ratio peak at ~0.25 for AF647 (more photons on the reflected pathway camera) and ~0.55 for CF680 (equal repartition on both cameras, Figure 2A). To retain an optimal number of localizations from both channels and ensure structural quality of the images, we assigned the ratios between 0.01 and 0.38 to AF647 and those between 0.42 and 0.99 to CF680, excluding 1.4% localizations outside of the selected ranges, and excluding the localizations only detected on a single camera (photon ratio of 0 or 1, which represents 33% and 10% of the total number of localizations on average in two-color acquisitions).

To assess the crosstalk between the two channels in this spectral demixing approach, we used the same three types of samples as for S2C-DNA-PAINT: nanorulers, sample labeled for a single target, or sample labeled for two targets. For the nanorulers experiment, we used the same short and long nanorulers as with S2C-DNA-PAINT: three spots spaced by 40 and 80 nm, respectively (Figure 2B). As these are DNA-PAINT samples conjugated to docking strands rather than organic fluorophores, we used an SD-DNA-PAINT imaging approach with two far-red imager strands: I1-Atto680 for the short nanoruler

(D) Adducin imaging done at constant 100% IF2-Atto643 imager concentration (blue), while varying the β2-spectrin IF1-Cy3B imager concentration (from 1% to 100%, orange).
(E) Autocorrelation curves from 1-μm-long intensity profiles along axons for the varying β2-spectrin-IF1-Cy3B (orange) and constant adducin-IF2-Atto643 (blue) channels for each imager concentration condition.
(F) Amplitude of the autocorrelation first peak for each imager concentration value. For (C) and (F), dots are individual axonal segments, error bars are SEM; stars show a significant difference with the 100%–1% condition (first bar) by post hoc Tukey-Kramer test, $p < 0.05$.

Please cite this article in press as: Friedl et al., Assessing crosstalk in simultaneous multicolor single-molecule localization microscopy, Cell Reports Methods (2023), https://doi.org/10.1016/j.crmeth.2023.100571

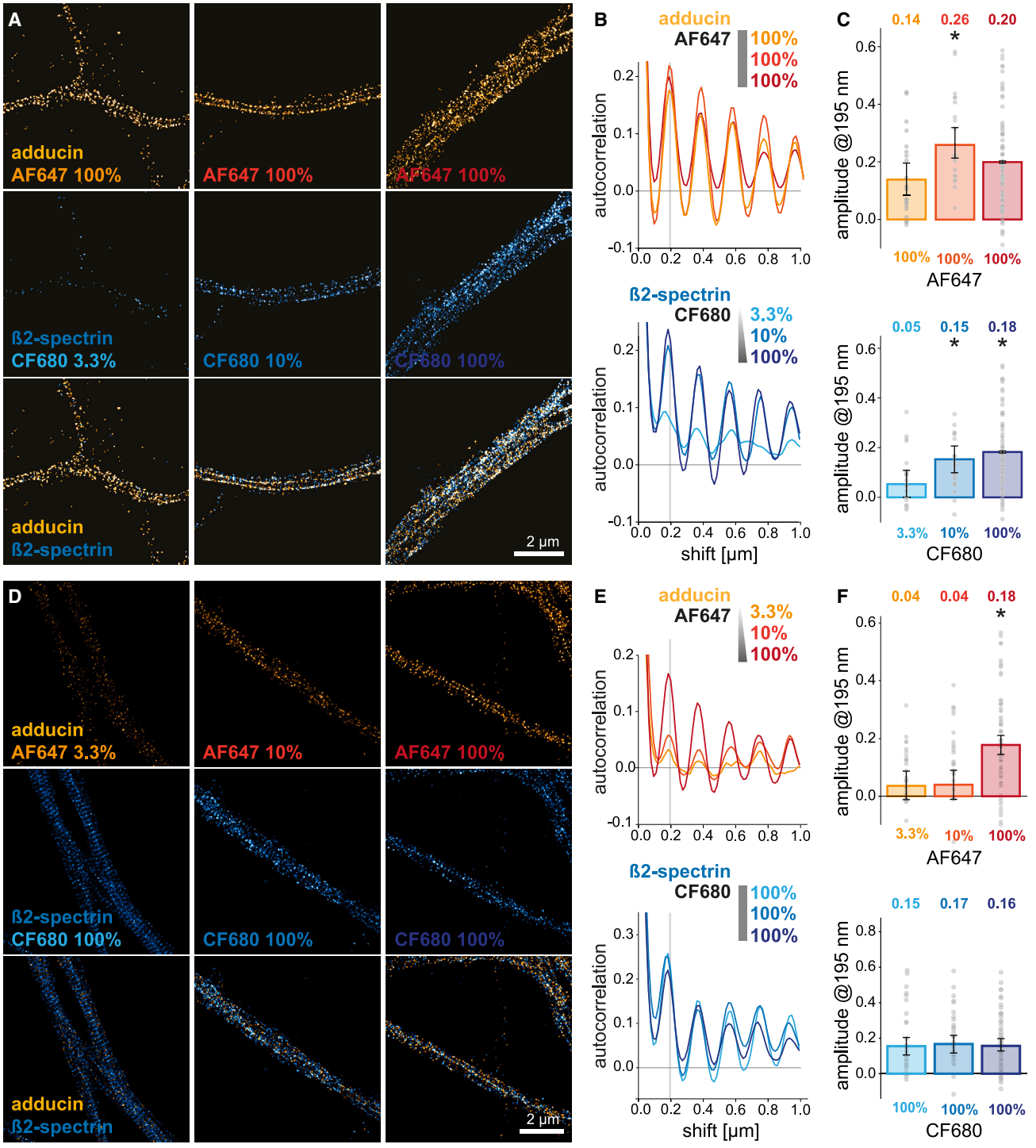

Figure 4. Effect of crosstalk on the detection of biologically relevant patterns by SD-dSTORM

(A) Reconstructed images of axons of stained for adducin (orange) and β2-spectrin (blue) imaged by SD-dSTORM using secondary antibodies conjugated with AF647 and CF680, respectively. During immunolabeling, the concentration of AF647-conjugated antibody was kept constant, while the concentration of CF680-conjugated antibody was increased successively from 3.3% to 10% and 100% of the total secondary antibody concentration.

(B) Autocorrelation curves from 1-µm-long intensity profiles along axons for the constant adducin-AF647 (orange) and varying β2-spectrin-CF680 (bottom) channels for each secondary antibody concentration condition.

(C) Amplitude of the autocorrelation first peak for each secondary antibody concentration value.

(legend continued on next page)

Please cite this article in press as: Friedl et al., Assessing crosstalk in simultaneous multicolor single-molecule localization microscopy, Cell Reports Methods (2023), https://doi.org/10.1016/j.crmeth.2023.100571

CellPress
OPEN ACCESS

(40 nm spaced, P1 docking strand) and I3-Atto655 for the long nanoruler (80 nm spaced, P3 docking strand); using fluorophores with slightly different spectra did not lead to significant difference in crosstalk values in our hands, and allowed us to use the same photon ratio range for demixing (0.01–0.38 for Atto655, 0.42–0.99 for Atto680) and crosstalk measurement (Figure 2B). This resulted in a crosstalk of 1.2% from Atto680 to Atto655, and 0.39% from Atto655 to Atto680 (Figure 2E).

For cellular imaging, we turned to spectral demixing dSTORM (SD-dSTORM), as several far-red fluorophores provide robust blinking under 640-nm illumination[28] and allow for faster acquisitions than DNA-PAINT. In spectral demixing approaches, all fluorophores appear on both cameras, hence there is no issue with adaptive SMLM algorithms picking up background in an "empty" channel. We thus could use the classical single-label imaging of COS-7 cells stained for microtubules and secondary antibodies conjugated to either AF647 or CF680 (Figure 2C). Photon ratios of single-target samples show a single peak around the expected ratio values (~0.25 for AF647 and ~0.55 for CF680), and we used the previously determined ratio ranges (0.01–0.38 for AF647, 0.42–0.99 for CF680). To estimate crosstalk, we segmented microtubules on the image from the target channel and counted localizations within this ROI in both channels (Figure 2C, bottom panels), then expressed crosstalk as the ratio of the localization number in the non-target channel over the sum of the localization numbers in the non-target and target channels. This resulted in a crosstalk of 0.72% from the CF680 channel into the AF647 channel, and of 0.46% from the AF647 channel into the CF680 channel (Figure 2E). Finally, we directly measured the crosstalk from two-color SD-dSTORM acquisition of samples labeled for microtubules (AF647-conjugated secondary antibodies) and clathrin (CF680-conjugated secondary antibody). The reconstructed images show a clean separation between the labeled structures (Figure 2D). As with S2C-DNA-PAINT, we estimated the crosstalk after generating single-target ROIs that excluded areas of overlap between microtubules and clathrin-coated pits (Figure S4). This resulted in a crosstalk of 4.6% from the CF680 channel to the AF647 channel, and 1.1% from the AF647 channel into the CF680 channel (Figure 2E).

Overall, we found that spectral demixing did not lead to more crosstalk compared with S2C-DNA-PAINT. On nanorulers, SD-dSTORM even results in lower crosstalk values than S2C-DNA-PAINT. This could be because spectral demixing filters out spurious localizations from background fluctuations that appear only on one camera, while S2C-DNA-PAINT cannot distinguish these localizations from real binding events, generating crosstalk. SD-dSTORM crosstalk on cellular samples is overall similar or higher than S2C-DNA-PAINT, probably due to the spectral overlap and the lower number of localizations that are collected compared with the repetitive binding in DNA-PAINT. Like for S2C-DNA-PAINT, we found the crosstalk from the higher-wavelength channel (Atto680/CF680) into the lower-wavelength channel (Atto655/AF647) to be slightly higher than in the other direction (lower wavelength into higher wavelength) for spectral demixing, as previously reported for the AF647/AF700 couple.[24] Both S2C-DNA-PAINT and SD-dSTORM are able to resolve the fine detail of cellular structures, as shown by the detection of hollow microtubule with an average gap between walls of 42 nm in S2C-DNA-PAINT and 36 nm in SD-dSTORM (Figures S6A–S6D). We further quantified the resolution of our images by estimating the localization precision using NeNa,[43] yielding values between 15 and 25 nm (Table S1).

Effect of crosstalk on the detection of biologically relevant patterns

To go further, we wanted to devise an experiment that could assess how crosstalk can perturb the visualization of biological structures, depending on the relative abundance of each target. For this, we turned to the membrane-associated periodic scaffold along the axon of neurons that is made of rings of adducin-associated actin spaced every 190 nm by a layer of spectrin tetramers, requiring super-resolution microscopy to be visible.[44,45] When hippocampal neurons in culture are labeled for adducin and the center of the spectrin tetramer (using an antibody binding near the carboxyterminus of β2-spectrin), this results in 190-nm periodic patterns of spectrin and adducin in antiphase, with spectrin bands and adducin bands alternating along the axon.[44,46] We reasoned that crosstalk from one target (for example adducin) into the other (spectrin) would directly perturb the measured periodicity of the latter, as it would result in the appearance of localization in-between the periodic bands. Furthermore, the labeling abundance of the spectrin and adducin being roughly similar in standard labeling conditions, we should be able to modulate the crosstalk by varying the labeling of one target (changing imager strand concentrations in PAINT of antibodies concentrations in dSTORM) and examine how this modulation affects the periodicity of the other target.

We thus labeled rat hippocampal neurons in culture for β2-spectrin and for adducin, and first imaged the resulting periodic patterns by S2C-DNA-PAINT: β2-spectrin revealed with an F1-conjugated secondary antibody and an IF1-Cy3B imager, adducin revealed with an F2-conjugated secondary antibody and an IF2-Atto643 imager (Figure 3). Two-color images were processed similarly to Figure 2E, with channel alignment by an affine transform (Figure S5). In the experiment shown in Figures 3A–3C, we repeatedly imaged the same sample by S2C-DNA-PAINT, keeping the β2-spectrin labeling constant with the IF1-Cy3B imager at its reference level (100%, i.e., 500 p.m., Figure 3A), and varying the abundance of the adducin labeling by using a rising concentration of IF2-Atto643 imager (1%: 6.25 p.m.; 10%: 62.5 p.m.; 100%: 625 p.m., Figure 3A). We measured the periodicity of each labeling by calculating the autocorrelation of

(D) β2-spectrin imaging done at constant 100% CF680-conjugated secondary antibody concentration (blue) while varying the adducin AF647-conjugated secondary antibody concentration (from 3.3% to 100%, orange).
(E) Autocorrelation curves from 1-μm-long intensity profiles along axons for the varying adducin-AF647 (orange) and constant β2-spectrin-CF680 (blue) channels for each secondary antibody concentration conditions.
(F) Amplitude of the autocorrelation first peak for each secondary antibody concentration value. For (C) and (F), dots are individual axonal segments, bars are SEM; stars show a significant difference compared with the first condition (left bar) by post hoc Tukey-Kramer test, $p < 0.05$.

Please cite this article in press as: Friedl et al., Assessing crosstalk in simultaneous multicolor single-molecule localization microscopy, Cell Reports Methods (2023), https://doi.org/10.1016/j.crmeth.2023.100571

intensity profiles along segments of axons (Figure 3B) and measuring the amplitude of the first peak at 190 nm[47] (see STAR Methods) (Figure 3C). Modulating the concentration of the IF2-Atto643 imager results in a gradual appearance of periodicity in the adducin channel, with the amplitude rising from 0.17 at 1% to 0.53 and 0.57 at 10% and 100%, respectively (Figures 3B and 3C, blue). Even at the maximum concentration, the adducin staining does not perturb the spectrin periodicity with an amplitude staying high at 0.6–0.7 (Figures 3B and 3C, yellow). In the reverse experiment, we varied the β2-spectrin labeling with a rising concentration IF1-Cy3B imager at its reference level (1%: 5 p.m.; 10%: 50 p.m.; 100%: 500 p.m., Figure 3D), and kept the adducin labeling constant (IF2-Atto643 imager concentration at 100%-625 p.m., Figure 3D). We were not always able to repeatedly image the same field of view (see Figure 3D), but this did not affect the analysis (see STAR Methods). The periodicity of the spectrin labeling was already apparent at 1% labeling, and at 100% labeling, spectrin labeling did not affect the periodicity of the adducin pattern (Figure 3E). In fact, the amplitude of the autocorrelation for adducin was lower (0.14) at 1% spectrin labeling, while it is unaffected by a switch between 10% and 100% spectrin labeling (0.28 and 0.30, respectively, Figure 3F). Statistics tests are summarized in Table S2. Overall, this shows that S2C-DNA-PAINT allows for imaging of biologically relevant patterns at the nanoscale, being robust to variations in the abundance of labeled proteins.

We next performed similar experiments using SD-dSTORM. Adducin and β2-spectrin were labeled by secondary antibodies conjugated with AF647 and CF680, respectively, and we imaged sister coverslips immunolabeled with a mix of unconjugated and fluorophore-conjugated secondary antibodies containing 3.3%, 10%, or 100% of conjugated antibody. We first kept the adducin-AF647 labeling constant at 100% and varied the β2-spectrin-CF680 labeling from 3.3% to 100% (Figures 4A–4C). β2-spectrin periodicity became robustly detectable at 10% and 100% labeling (Figure 4C, blue). Adducin-AF647 periodicity, while kept at 100% labeling, shows variations with a higher value for the middle concentration of β2-spectrin-CF680, but no difference between the two extremes (3.3% and 100%), making it unlikely that crosstalk is influencing the observed periodicity (Figure 4C, yellow). In the reverse experiment, we kept the β2-spectrin-CF680 labeling constant at 100% and varied the adducin-AF647 labeling from 3.3% to 100% (Figures 4D–4F). Here again, we detected a rise in the periodicity of the pattern for adducin between 3.3% and 100% (Figure 4E, yellow). Meanwhile, the β2-spectrin-CF680 periodicity remained constant when increasing the adducin labeling density (Figure 4E, blue), indicating that crosstalk is low enough to not perturb the periodicity assessment. In conclusion, we could not detect a detrimental effect of a dense labeling in one channel to the quantitative assessment of the labeling in the other channel in both S2C-DNA-PAINT and SD-dSTORM, demonstrating that the two approaches allow investigation of biologically relevant structures in a robust manner.

Both S2C-DNA-PAINT and SD-dSTORM are compatible with astigmatism-based 3D SMLM

We next assessed if the two approaches can be combined with 3D SMLM via the insertion of a cylindrical lens in front of each camera to induce astigmatism in the PSF[48–50] (Figure S1). We evaluated both S2C-DNA-PAINT and SD-dSTORM approaches using COS-7 cells labeled for microtubules and clathrin.[42] For S2C-DNA-PAINT using Atto643 and Cy3B-conjugated imagers, we obtained good structural quality for both channels (Figure 5A). Ratiometric analysis shows that simultaneous two-color, 3D acquisitions yield similar results to the 2D case (see Figure 1A) with most events localized only on one camera, allowing for a straightforward separation between channels (Figure 5B). We generated XZ sections along three microtubules and registered them to obtain an average microtubule profile (Figure 5C), and calculated the microtubule section full-width at half-maximum (FWHM) in the X and Z directions to be 68 and 110 nm, respectively.

For SD-dSTORM using AF647 and CF680-conjugated secondary antibodies, we also obtained good structural quality for both channels together with Z localization across the focal plane (Figure 5D). Ratiometric analysis provided a distribution of photon ratios similar to the 2D case (see Figure 2A), with an AF647 peak at ∼0.25 and a CF680 peak at ∼0.55, allowing use of the previously determined ratio ranges to separate the two channels (Figure 5E). Averaging and analysis of microtubule cross-sections yielded an FWHM of 61 nm in both X and Z directions (Figure 5F), values similar to previously reported thickness[27] and lower than the average thickness we obtained by S2C-DNA-PAINT. PAINT has been shown to result in thicker shells around microtubules,[51] and in our case the much higher thickness in Z might be due to sub-optimal vertical drift correction, as DNA-PAINT acquisitions are significantly longer than STORM ones (Table S1).

SD-dSTORM extension to simultaneous three-target imaging

SD-dSTORM can readily be extended to more than two colors,[20–22] with a currently preferred use of three far-red fluorophores excited by a single laser (AF647, CF660C, and CF680).[29,32,36] We thus extended our SD-dSTORM crosstalk analysis to three-color imaging using these fluorophores (Figure 6A). To assess the crosstalk between each channel, we used two types of cellular samples previously validated for two-color SD-dSTORM: COS-7 cells labeled for microtubules using a single fluorophore (AF647, CF660C, or CF680, Figures 6B and 6C), or labeled for three targets using each of these fluorophores (Figures 6D and 6E). Single-target labeled samples allowed us to obtain the photon ratio distribution for each fluorophore: AF647 and CF680 still had peaks at photon ratios of ∼0.25 and 0.55, respectively, and CF660C peak was at a photon ratio of ∼0.35 (Figure 6B). From these distributions, we defined ratio ranges for each channel: 0.01–0.29 for AF647, 0.31–0.40 for CF660C, and 0.50–0.99 for CF680 (Figure 6B). From the resulting single-color images (Figure 6C), we could measure the number of localizations in the non-target channels from ROIs defined on the target channel to calculate crosstalk values (Figure 6F). We found that AF647 crosstalk into CF660C and CF680 was 8.4% and 0.42%, respectively; that CF660C crosstalk into AF647 and CF680 was 8.4% and 3.3%, respectively; and that CF680 crosstalk into AF647 and CF660C was 0.70% and 2.8%, respectively (Figure 6F). We then turned to simultaneous imaging of three targets using COS-7 cells labeled for the endoplasmic reticulum (ER)

Cell Reports Methods
Article

CellPress
OPEN ACCESS

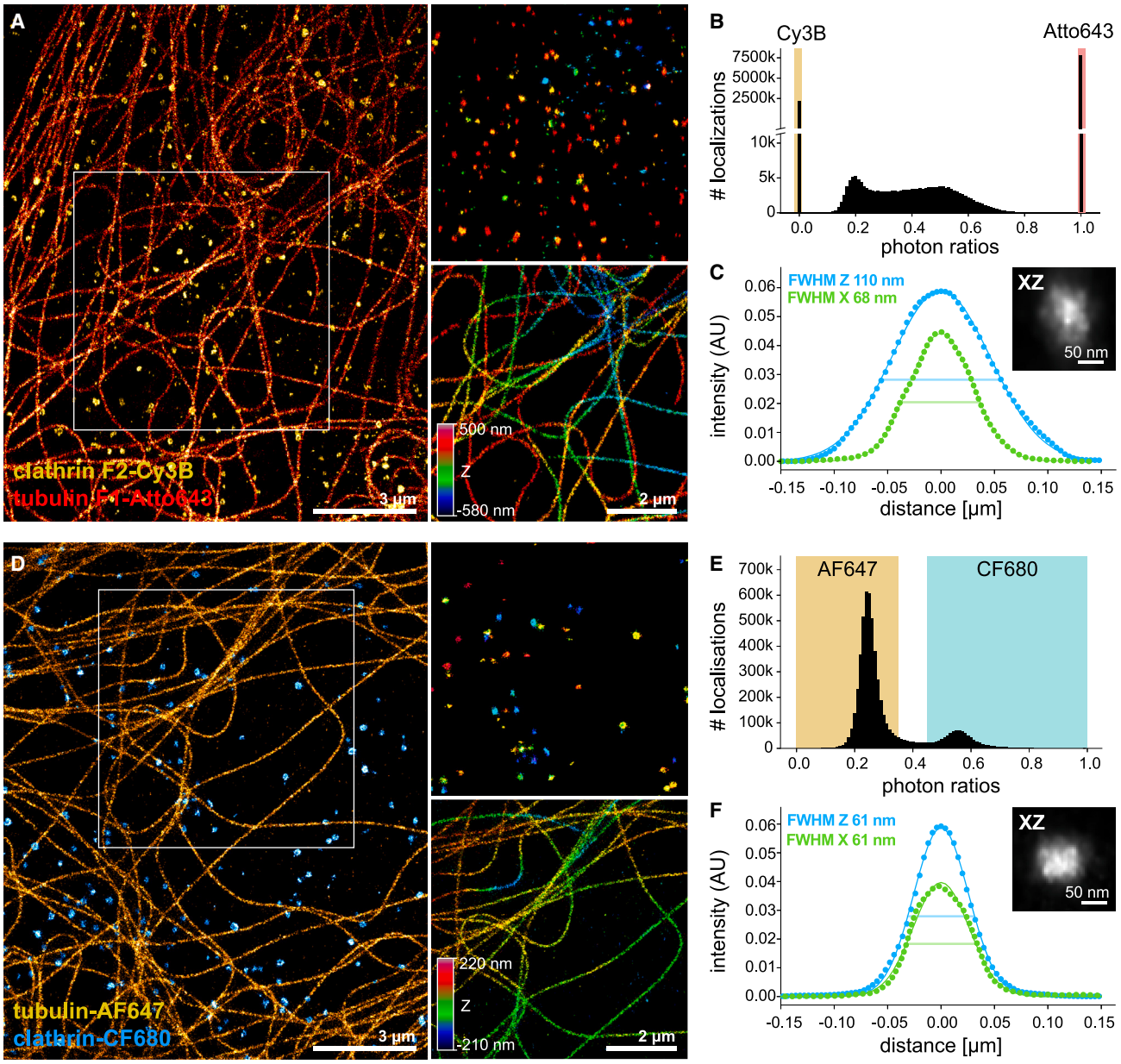

Figure 5. Extension of S2C-DNA-PAINT and SD-dSTORM to astigmatism-based 3D SMLM

(A) 3D S2C-DNA-PAINT: image of a COS-7 cell labeled for clathrin and tubulin, imaged with IF2-Cy3B (orange) and IF1-Atto643 (red), respectively. Insets show zoomed isolated channels, color-coded for Z.

(B) Distribution of the photon ratios for the acquisition in (A), with colored areas for the ratios chosen for demixing: 0–0.01 for Cy3B (orange), 0.99–1 for Atto643 (red).

(C) Full-width half-maximum (FWHM) analysis of the average intensity profile for transverse section along three isolated microtubules in (A). Inset, average transverse section obtained after alignment of individual sections.

(D) SD-dSTORM image of a COS-7 cell labeled for tubulin and clathrin, revealed with secondary antibodies conjugated to AF647 (yellow) and CF680 (cyan), respectively. Insets show zoomed isolated channels, color-coded for Z.

(E) Distribution of the photon ratios for the acquisition in (A), with colored areas for the ratios chosen for demixing: 0.01–0.38 for AF647 (yellow area), 0.42–0.99 for CF680 (blue area).

(F) FWHM analysis of the average intensity profile for transverse section along three isolated microtubules in (A). Inset, average transverse section obtained after alignment of individual sections.

Please cite this article in press as: Friedl et al., Assessing crosstalk in simultaneous multicolor single-molecule localization microscopy, Cell Reports Methods (2023), https://doi.org/10.1016/j.crmeth.2023.100571

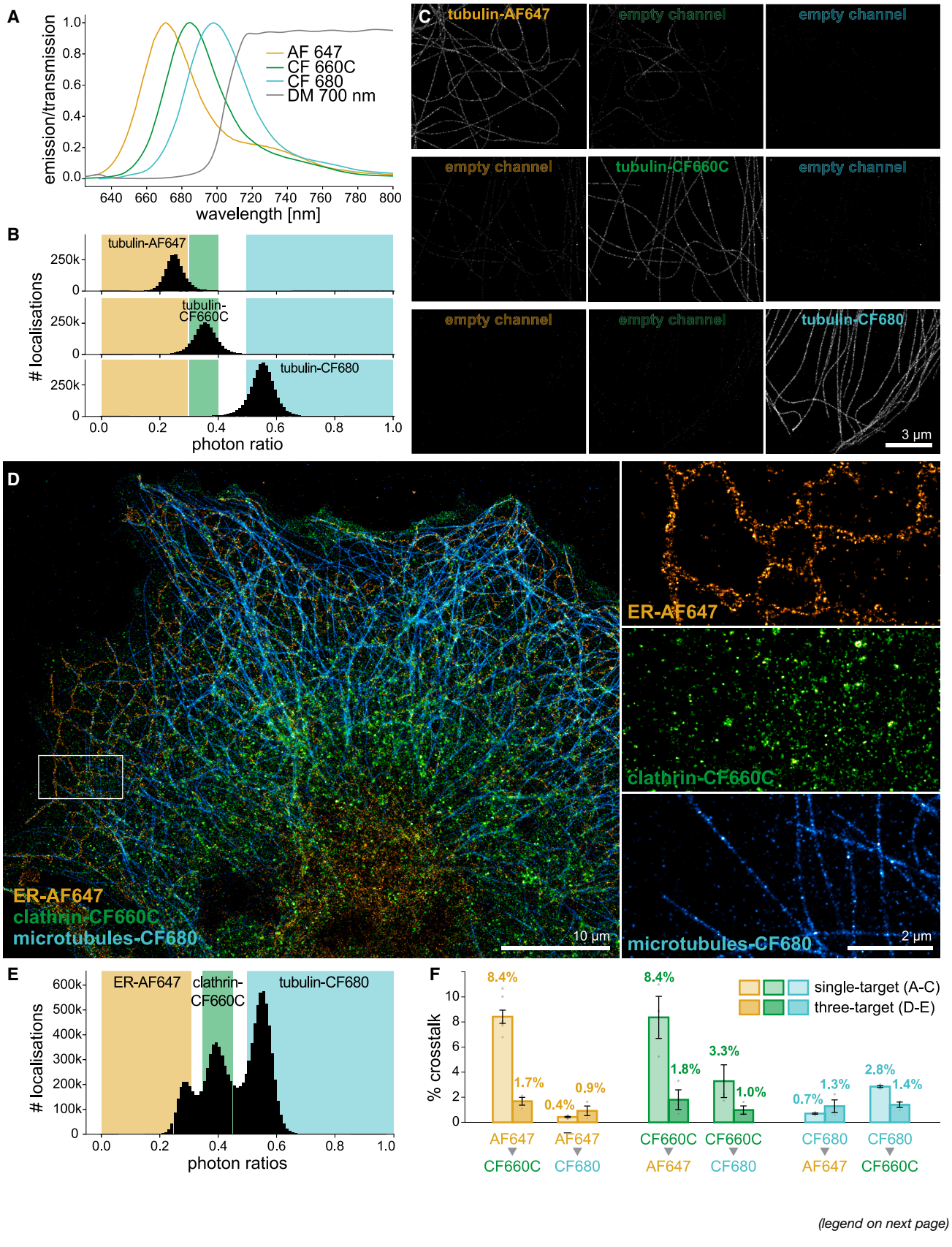

(legend on next page)

Please cite this article in press as: Friedl et al., Assessing crosstalk in simultaneous multicolor single-molecule localization microscopy, Cell Reports Methods (2023), https://doi.org/10.1016/j.crmeth.2023.100571

(anti-rtn4b antibody) with AF647, clathrin with CF660C, and microtubules with CF680 (Figure 6D). For these three-color acquisitions, we found that the photon ratio peak for CF660C could shift by up to ~0.05 depending on the acquired sequence, and we accordingly adjusted the photon ratio ranges for demixing (Figure 6E). Single-channel images demonstrate the good structural quality of the images for each structure, although the clathrin staining was not as good as with the glutaraldehyde fixation used for two-color labeling (Figure 6D, right). For rtn4b labeling along the ER, we could measure an average distance of ~100 nm between its concentration along opposing walls, consistent with recent SMLM results[52] (Figures S6E–S6G). The same exclusive ROI strategy as in the two-color case, this time combining the three targets, was used to estimate the crosstalk directly from three-color images. Interestingly, these led to lower values than the single-target experiments: we found that AF647 crosstalk into CF660C and CF680 was 1.7% and 0.92%, respectively; that CF660C crosstalk into AF647 and CF680 was 1.8% and 0.98%, respectively; and that CF680 crosstalk into AF647 and CF660C was 1.3% and 1.4%, respectively (Figure 6E). Despite these lower values, the crosstalk estimation obtained from three-color images was consistent, with similar values in both directions for each fluorophore pair, and considering the photon ratio distribution where the AF647 and CF660C are closer to one another (higher crosstalk) than CF660C and CF680 (lower crosstalk).

DISCUSSION

In this work, we used two approaches for simultaneous multicolor SMLM. In the first approach, we split the emission of two spectrally distinct red and far-red fluorophores each excited by one light source, a setup similar to multicolor confocal microscopy that we expected to result in a low crosstalk between channels.[15,16] The second approach is based on demixing two far-red fluorophores excited by a single laser, with blinking events appearing with a different balance of intensities on each camera after splitting by a well-chosen dichroic mirror. This SD-dSTORM method was devised in the early days of SMLM,[20–25] and has since become a favorite option for home-made single molecule microscope builders and users[29,30,53,54] as it allows for two- to three-color imaging with good quality across channels together with low chromatic aberration.[55]

Despite its advantages, SMLM users often have the perception that SD-dSTORM would be more susceptible to crosstalk between channels than the classical two-color approach. We thus set up to rigorously measure and compare the crosstalk of SD-dSTORM with the baseline crosstalk of S2C-DNA-PAINT using three different types of samples. The first type consists of two DNA origami nanorulers of different sizes seeded on the same coverslip.[40,41] Our idea was to create a sample where each target would be fully separated spatially and identifiable by its shape without relying on color/channel information. This would provide an unbiased assessment of crosstalk from a standard multicolor acquisition. The nanoruler samples provided values below 2% for crosstalk in S2C-DNA-PAINT (1.7% and 1.3%) and slightly lower for SD-DNA-PAINT (1.2% and 0.39%). This suggests that crosstalk from the spectral demixing procedure is low, and smaller than the crosstalk arising from spurious detections within each channel in S2C-DNA-PAINT.

The second type of samples are cells labeled for a single target using each of the fluorophores used. This is a straightforward and widely used approach to estimate crosstalk. However, when evaluating the S2C-DNA-PAINT approach where the blinking event appears only on one camera, we realized that state-of-the-art SMLM algorithms based on an adaptive thresholding to detect blinking events introduces a significant bias in this approach, detecting a lot of background fluctuation events in the channel with no signal. We thus devised a crosstalk evaluation procedure for S2C-DNA-PAINT taking advantage of the possibility of performing successive acquisitions of the same field of view with different imager mixtures. We were able to measure the change induced in a non-target channel by the presence of signal in the other channel, while compensating each for background. This approach yielded very low values for the S2C-DNA-PAINT crosstalk between Cy3B and Atto643 (0.4% and 0.02% for each direction): this is consistent with the idea that the main source of apparent crosstalk in S2C-DNA-PAINT does not come from optical sources, but from non-specific imager binding and detection during imaging. For SD-dSTORM, blinking events appear on both cameras, allowing for a straightforward single-target strategy even when using an adaptive algorithm. The single-target samples yielded 0.7% and 0.5% for CF680 to AF647 and for AF647 to CF680, respectively. These values are lower than the nanoruler-based values (1.2% and 0.39%), suggesting that this simple single target-based crosstalk measurement is optimistic. Indeed, the absence of a second fluorophore avoids contribution from its non-specific labeling, and the reduction in blinking density on the two cameras results in less bias from overlapping fluorophores. On two-target cellular samples, the estimation of the crosstalk is logically higher, even after careful

Figure 6. Extension of SD-dSTORM to three targets and crosstalk evaluation

(A) Emission spectra of the fluorophores used for three-color SD-dSTORM: AF647 (yellow), CF660C (green), and CF680 (blue), and transmission of the 700-nm long-pass dichroic inserted in the detection pathway (gray).

(B) Photon ratios for each fluorophore determined by ratiometric analysis from single-fluorophore-stained microtubules in COS-7 cells. Colored areas highlight the ratio ranges chosen for AF647 (0.01–0.29, yellow), CF660C (0.31–0.40, green), and CF680 (0.50–0.99, blue).

(C) SD-dSTORM images of COS cells stained for microtubules using secondary antibodies conjugated to AF647 (yellow), CF660C (green), or CF680 (blue). ROIs segmented from the microtubule channel were used to measure the number of localizations in each channel and calculate the crosstalk between channels.

(D) Three-channel SD-dSTORM image of a COS cell labeled for the endoplasmic reticulum (ER; AF647), clathrin (CF660C), and tubulin (CF680). Insets show zoomed isolated channels.

(E) Photon ratios for each fluorophore from the three-channel acquisition in (D). Colored areas highlight the ratio ranges chosen to demix AF647 (0.01–0.30, yellow), CF660C (0.35–0.45, green), and CF680 (0.50–0.99, blue).

(F) Crosstalk between the channels calculated from the single-fluorophore staining (C) and the three-target staining (D) cellular samples. For the three-target sample, exclusive ROIs were used to delineate regions containing one target, but not the two others. Points correspond to individual images or datapoints; error bars are SEM.

Please cite this article in press as: Friedl et al., Assessing crosstalk in simultaneous multicolor single-molecule localization microscopy, Cell Reports Methods (2023), https://doi.org/10.1016/j.crmeth.2023.100571

segmentation of cellular structures and subtraction to avoid overlapping structures: we obtained crosstalk estimations of 2.1% and 1.4% in S2C-DNA-PAINT (Figure 1), and 4.6% and 1.1% in SD-dSTORM. Here biases from non-specific labeling, structure complexity, and blinking event overlap, likely all participate in higher crosstalk values.

From these experiments, what would be the best way to estimate crosstalk in simultaneous multicolor SMLM experiments? Single-target sample methods cannot be performed in the same way in DNA-PAINT and dSTORM, making comparison difficult, while two-color samples are biased by structure and fluorophore overlap. The two-color nanorulers sample we introduce in this work might be a better approach: it provides a crosstalk estimation in the realistic presence of the two fluorophores, with clearly distinct structures that don't overlap and can be identified by their shape independently of their detection in the two channels. In order for this sample to become standard, two-color nanoruler samples should be made readily available with either DNA docking strands for PAINT and conjugated fluorophores for dSTORM.

In addition to assessing the crosstalk on different types of samples, we also tried to evaluate how it could affect the results of experiments by interfering with a known biological pattern. Usually, crosstalk is evaluated by comparing the same target across channels (single-target samples) or target with similar abundance (microtubule and clathrin in our two-target samples). However, crosstalk is likely to be more detrimental in experiments where one target has a low abundance compared with the other. To assess this, we took advantage of neuronal axons where two proteins (β2-spectrin and adducin) show a similar labeling density with a complementary, 190-nm periodic staining pattern[44,45]: we could assess if modulating the labeling density of one target would affect the other target. Interestingly, in both S2C-DNA-PAINT and SD-dSTORM, we did not detect a detrimental influence between an increasing labeling density in one channel on the other channel.

Finally, we confirmed that both S2C-DNA-PAINT and SD-dSTORM can readily be extended to astigmatism-based 3D SMLM, with no alteration in the image quality or channel separation (see Figure 5), and showed how SD-dSTORM can be extended to three colors (see Figure 6).[29,32,36] However, one advantage of SD-dSTORM is that the specificity can be optimized by tuning the photon ratio ranges for each channel, to the cost of more rejected localizations and a sparser image. Overall, our experiments show that spectral demixing does not result in a significantly higher crosstalk, compared with simultaneous spectrally separated acquisitions, with overall crosstalk values around 1%–2%. Refinements in channel assignment in SD-dSTORM[32,33,36] might allow for an even better performance of spectral demixing approaches. The robustness of spectral demixing SMLM to crosstalk validates this approach for the meaningful interrogation of nanoscale structures in their cellular context.

Beyond crosstalk, a prevalent disadvantage of SMLM is its low throughput. One way to optimize the "localization throughput" of an SMLM experiment is to get as close as possible to the maximum blinking density that the processing algorithm can handle, with higher fractions of active fluorophores in dSTORM or higher binding rates of imager strands in DNA-PAINT. In this regard, spectral demixing strategies are lowering the maximal attainable density by superimposing the fluorophores imaged on each camera frame. Yet for the two optimized strategies we tested here, two-color SD-dSTORM is not slower than S2C-DNA-PAINT, because the loss in maximum density is more than compensated by the faster blinking and lower exposure times possible with dSTORM compared with DNA-PAINT (Table S1). For two-color acquisitions, we thus would favor SD-dSTORM over S2C-DNA-PAINT as it is compatible with initial observation before super-resolved acquisition, faster, straightforward to implement with a commercially available setup,[56–58] and readily extensible to three-color imaging. A key advantage of S2C-DNA-PAINT in the future is that implementing successive rounds of PAINT imaging would provide a straightforward way to extend it to multiplexing with four or more channels, with the possibility of combining it with recent faster DNA-PAINT approaches[16,59] for a significant gain in speed compared with single-color exchange-PAINT.

Limitations of the study

The distinct source of blinking in DNA-PAINT and dSTORM requires distinct fluorophore pairs, introducing a necessary variation in our comparison. The two-color nanoruler sample generates a low number of localizations—having bulkier structures providing a larger number of blinking events would help to make this method more robust, alleviating the manual selection of fully reconstructed nanorulers we used here.

STAR★METHODS

Detailed methods are provided in the online version of this paper and include the following:

- KEY RESOURCES TABLE
- RESOURCE AVAILABILITY
  - Lead contact
  - Materials availability
  - Data and code availability
- EXPERIMENTAL MODEL AND STUDY PARTICIPANT DETAILS
  - COS-7 cell culture
  - Neuron culture
- METHOD DETAILS
  - COS-7 fixation
  - Neuronal fixation
  - Immunostaining and antibodies
  - SMLM microscope
  - DNA-PAINT acquisition
  - Spectral demixing-STORM acquisition
  - Nanorulers sample and imaging
  - SMLM data processing
  - Channel assignment (demixing) from two-camera data
  - R = I(*trans*)/I(*trans*) + I(*refl*)
- QUANTIFICATION AND STATISTICAL ANALYSIS
  - Crosstalk analysis
  - Analysis of the actin/spectrin periodicity along axons
  - Microtubule cross-section analysis

- Microtubule and endoplasmic reticulum 2D profile analysis
- Estimation of localization precision with NeNa

SUPPLEMENTAL INFORMATION

Supplemental information can be found online at https://doi.org/10.1016/j.crmeth.2023.100571.

ACKNOWLEDGMENTS

We would like to acknowledge funding by the Agence Nationale de la Recherche ANR-20-CE16-021-03 to C.L.; the Fédération pour la Recherche sur le Cerveau (AOE 16 "Espoir en tête" 2021) to C.L.; ANR-21-CE42-0015 to N.B., S.L.F., and C.L.; and the Association Nationale de la Recherche et de la Technologie (ANRT) for the co-funding of K.F. and A.M. (CIFRE PhD). This work has received funding from the European Union's Horizon 2020 research and innovation programme under grant agreement #871124 Laserlab-Europe (JRA ALTIS). We would like to thank Marie-Jeanne Papandréou for discussions.

AUTHOR CONTRIBUTIONS

Conceptualization, all authors; methodology, all authors; formal analysis, K.F. and A.M.; investigation, K.F.; resources, F.B.R., V.C., and N.B.; writing – original draft, K.F. and C.L.; writing – review and editing, all authors; visualization, K.F., C.L., and A.M.; supervision and project administration, C.L.; funding acquisition, N.B., S.L.F., and C.L.

DECLARATION OF INTERESTS

K.F., A.M., V.C., and N.B. are employees of Abbelight. N.B. and S.L.F. are shareholders of Abbelight.

Received: January 23, 2023
Revised: July 3, 2023
Accepted: August 4, 2023
Published: September 1, 2023

REFERENCES

1. Vangindertael, J., Camacho, R., Sempels, W., Mizuno, H., Dedecker, P., and Janssen, K.P.F. (2018). An introduction to optical super-resolution microscopy for the adventurous biologist. Methods Appl. Fluoresc. *6*, 022003. https://doi.org/10.1088/2050-6120/aaae0c.
2. Jacquemet, G., Carisey, A.F., Hamidi, H., Henriques, R., and Leterrier, C. (2020). The cell biologist's guide to super-resolution microscopy. J. Cell Sci. *133*, jcs240713. https://doi.org/10.1242/jcs.240713.
3. Sauer, M., and Heilemann, M. (2017). Single-Molecule Localization Microscopy in Eukaryotes. Chem. Rev. *117*, 7478–7509. https://doi.org/10.1021/acs.chemrev.6b00667.
4. Lelek, M., Gyparaki, M.T., Beliu, G., Schueder, F., Griffié, J., Manley, S., Jungmann, R., Sauer, M., Lakadamyali, M., and Zimmer, C. (2021). Single-molecule localization microscopy. Nat. Rev. Methods Primers *1*, 39. https://doi.org/10.1038/s43586-021-00038-x.
5. Liu, S., Hoess, P., and Ries, J. (2022). Super-Resolution Microscopy for Structural Cell Biology. Annu. Rev. Biophys. *51*, 301–326. https://doi.org/10.1146/annurev-biophys-102521-112912.
6. Deschout, H., Cella Zanacchi, F., Mlodzianoski, M., Diaspro, A., Bewersdorf, J., Hess, S.T., and Braeckmans, K. (2014). Precisely and accurately localizing single emitters in fluorescence microscopy. Nat. Methods *11*, 253–266. https://doi.org/10.1038/nmeth.2843.
7. Heilemann, M., van de Linde, S., Schüttpelz, M., Kasper, R., Seefeldt, B., Mukherjee, A., tinnefeld, P., and Sauer, M. (2008). Subdiffraction-resolution fluorescence imaging with conventional fluorescent probes. Angew. Chem., Int. Ed. Engl. *47*, 6172–6176. https://doi.org/10.1002/anie.200802376.
8. Rust, M.J., Bates, M., and Zhuang, X. (2006). Sub-diffraction-limit imaging by stochastic optical reconstruction microscopy (STORM). Nat. Methods *3*, 793–795. https://doi.org/10.1038/nmeth929.
9. Jungmann, R., Avendaño, M.S., Woehrstein, J.B., Dai, M., Shih, W.M., and Yin, P. (2014). Multiplexed 3D cellular super-resolution imaging with DNA-PAINT and Exchange-PAINT. Nat. Methods *11*, 313–318. https://doi.org/10.1038/nmeth.2835.
10. Agasti, S.S., Wang, Y., Schueder, F., Sukumar, A., Jungmann, R., and Yin, P. (2017). DNA-barcoded labeling probes for highly multiplexed Exchange-PAINT imaging. Chem. Sci. *8*, 3080–3091. https://doi.org/10.1039/c6sc05420j.
11. Guo, S.-M., Veneziano, R., Gordonov, S., Li, L., Danielson, E., Perez de Arce, K., Park, D., Kulesa, A.B., Wamhoff, E.-C., Blainey, P.C., et al. (2019). Multiplexed and high-throughput neuronal fluorescence imaging with diffusible probes. Nat. Commun. *10*, 4377. https://doi.org/10.1038/s41467-019-12372-6.
12. Schueder, F., Stein, J., Stehr, F., Auer, A., Sperl, B., Strauss, M.T., Schwille, P., and Jungmann, R. (2019). An order of magnitude faster DNA-PAINT imaging by optimized sequence design and buffer conditions. Nat. Methods *16*, 1101–1104. https://doi.org/10.1038/s41592-019-0584-7.
13. Strauss, S., and Jungmann, R. (2020). Up to 100-fold speed-up and multiplexing in optimized DNA-PAINT. Nat. Methods *17*, 789–791. https://doi.org/10.1038/s41592-020-0869-x.
14. Civitci, F., Shangguan, J., Zheng, T., Tao, K., Rames, M., Kenison, J., Zhang, Y., Wu, L., Phelps, C., Esener, S., and Nan, X. (2020). Fast and multiplexed superresolution imaging with DNA-PAINT-ERS. Nat. Commun. *11*, 4339. https://doi.org/10.1038/s41467-020-18181-6.
15. Cheng, J., Allgeyer, E.S., Richens, J.H., Dzafic, E., Palandri, A., Lewków, B., Sirinakis, G., and St Johnston, D. (2021). A single molecule localization microscopy method for tissues reveals nonrandom nuclear pore distribution in Drosophila. J. Cell Sci. *134*, jcs259570. https://doi.org/10.1242/jcs.259570.
16. Chung, K.K.H., Zhang, Z., Kidd, P., Zhang, Y., Williams, N.D., Rollins, B., Yang, Y., Lin, C., Baddeley, D., and Bewersdorf, J. (2022). Fluorogenic DNA-PAINT for faster, low-background super-resolution imaging. Nat. Methods *19*, 554–559. https://doi.org/10.1038/s41592-022-01464-9.
17. Øvrebø, Ø., Ojansivu, M., Kartasalo, K., Barriga, H.M.G., Ranefall, P., Holme, M.N., and Stevens, M.M. (2023). RegiSTORM: channel registration for multi-color stochastic optical reconstruction microscopy. BMC Bioinf. *24*, 237. https://doi.org/10.1186/s12859-023-05320-1.
18. Erdelyi, M., Rees, E., Metcalf, D., Schierle, G.S.K., Dudas, L., Sinko, J., Knight, A.E., and Kaminski, C.F. (2013). Correcting chromatic offset in multicolor super-resolution localization microscopy. Opt Express *21*, 10978–10988. https://doi.org/10.1364/oe.21.010978.
19. Martens, K.J.A., Turkowyd, B., and Endesfelder, U. (2022). Raw Data to Results: A Hands-On Introduction and Overview of Computational Analysis for Single-Molecule Localization Microscopy. Front. Bioinform. *1*. https://doi.org/10.3389/fbinf.2021.817254.
20. Bossi, M., Fölling, J., Belov, V.N., Boyarskiy, V.P., Medda, R., Egner, A., Eggeling, C., Schönle, A., and Hell, S.W. (2008). Multicolor Far-Field Fluorescence Nanoscopy through Isolated Detection of Distinct Molecular Species. Nano Lett. *8*, 2463–2468. https://doi.org/10.1021/nl801471d.
21. Testa, I., Wurm, C.A., Medda, R., Rothermel, E., von Middendorf, C., Eggeling, C., Fölling, J., Jakobs, S., Schönle, A., Hell, S.W., and Eggeling, C. (2010). Multicolor fluorescence nanoscopy in fixed and living cells by exciting conventional fluorophores with a single wavelength. Biophys. J. *99*, 2686–2694. https://doi.org/10.1016/j.bpj.2010.08.012.
22. Baddeley, D., Crossman, D., Rossberger, S., Cheyne, J.E., Montgomery, J.M., Jayasinghe, I.D., Cremer, C., Cannell, M.B., and Soeller, C. (2011). 4D super-resolution microscopy with conventional fluorophores and single wavelength excitation in optically thick cells and tissues. PLoS One *6*, e20645. https://doi.org/10.1371/journal.pone.0020645.g004.

23. Gunewardene, M.S., Subach, F.V., Gould, T.J., Penoncello, G.P., Gudheti, M.V., Verkhusha, V.V., and Hess, S.T. (2011). Superresolution imaging of multiple fluorescent proteins with highly overlapping emission spectra in living cells. Biophys. J. *101*, 1522–1528. https://doi.org/10.1016/j.bpj.2011.07.049.

24. Lampe, A., Haucke, V., Sigrist, S.J., Heilemann, M., and Schmoranzer, J. (2012). Multi-colour direct STORM with red emitting carbocyanines. Biol. Cell. *104*, 229–237. https://doi.org/10.1111/boc.201100011.

25. Schönle, A., and Hell, S.W. (2007). Fluorescence nanoscopy goes multicolor. Nat. Biotechnol. *25*, 1234–1235. https://doi.org/10.1038/nbt1107-1234.

26. Platonova, E., Winterflood, C.M., and Ewers, H. (2015). A Simple Method for GFP- and RFP-based Dual Color Single-Molecule Localization Microscopy. ACS Chem. Biol. *10*, 1411–1416. https://doi.org/10.1021/acschembio.5b00046.

27. Winterflood, C.M., Platonova, E., Albrecht, D., and Ewers, H. (2015). Dual-Color 3D Superresolution Microscopy by Combined Spectral-Demixing and Biplane Imaging. Biophys. J. *109*, 3–6. https://doi.org/10.1016/j.bpj.2015.05.026.

28. Lehmann, M., Lichtner, G., Klenz, H., and Schmoranzer, J. (2016). Novel organic dyes for multicolor localization-based super-resolution microscopy. J. Biophot. *9*, 161–170. https://doi.org/10.1002/jbio.201500119.

29. Favuzzi, E., Marques-Smith, A., Deogracias, R., Winterflood, C.M., Sánchez-Aguilera, A., Mantoan, L., Maeso, P., Fernandes, C., Ewers, H., and Rico, B. (2017). Activity-Dependent Gating of Parvalbumin Interneuron Function by the Perineuronal Net Protein Brevican. Neuron *95*, 639–655.e10. https://doi.org/10.1016/j.neuron.2017.06.028.

30. Gorur, A., Yuan, L., Kenny, S.J., Baba, S., Xu, K., and Schekman, R. (2017). COPII-coated membranes function as transport carriers of intracellular procollagen I. J. Cell Biol. *216*, 1745–1759. https://doi.org/10.1083/jcb.201702135.

31. Zhang, Y., Schroeder, L.K., Lessard, M.D., Kidd, P., Chung, J., Song, Y., Benedetti, L., Li, Y., Ries, J., Grimm, J.B., et al. (2020). Nanoscale subcellular architecture revealed by multicolor three-dimensional salvaged fluorescence imaging. Nat. Methods *17*, 225–231. https://doi.org/10.1038/s41592-019-0676-4.

32. Andronov, L., Genthial, R., Hentsch, D., and Klaholz, B.P. (2022). splitSMLM, a spectral demixing method for high-precision multi-color localization microscopy applied to nuclear pore complexes. Commun. Biol. *5*, 1100. https://doi.org/10.1038/s42003-022-04040-1.

33. Siemons, M.E., Jurriens, D., Smith, C.S., and Kapitein, L.C. (2022). 3D multi-color far-red single-molecule localization microscopy with probability-based fluorophore classificationPrerint at. bioRxiv. https://doi.org/10.1101/2022.01.14.476290.

34. Gimber, N., Strauss, S., Jungmann, R., and Schmoranzer, J. (2022). Simultaneous Multicolor DNA-PAINT without Sequential Fluid Exchange Using Spectral Demixing. Nano Lett. *22*, 2682–2690. https://doi.org/10.1021/acs.nanolett.1c04520.

35. Tadeus, G., Lampe, A., and Schmoranzer, J. (2015). SDmixer—a versatile software tool for spectral demixing of multicolor single molecule localization data. Methods Appl. Fluoresc. *3*, 037001. https://doi.org/10.1088/2050-6120/3/3/037001.

36. Li, Y., Shi, W., Liu, S., Cavka, I., Wu, Y.-L., Matti, U., Wu, D., Koehler, S., and Ries, J. (2022). Global fitting for high-accuracy multi-channel single-molecule localization. Nat. Commun. *13*, 3133. https://doi.org/10.1038/s41467-022-30719-4.

37. Mau, A., Friedl, K., Leterrier, C., Bourg, N., and Lévêque-Fort, S. (2021). Fast widefield scan provides tunable and uniform illumination optimizing super-resolution microscopy on large fields. Nat. Commun. *12*, 3077. https://doi.org/10.1038/s41467-021-23405-4.

38. Dempsey, G.T., Vaughan, J.C., Chen, K.H., Bates, M., and Zhuang, X. (2011). Evaluation of fluorophores for optimal performance in localization-based super-resolution imaging. Nat. Methods *8*, 1027–1036. https://doi.org/10.1038/nmeth.1768.

39. Schnitzbauer, J., Strauss, M.T., Schlichthaerle, T., Schueder, F., and Jungmann, R. (2017). Super-resolution microscopy with DNA-PAINT. Nat. Protoc. *12*, 1198–1228. https://doi.org/10.1038/nprot.2017.024.

40. Lin, R., Clowsley, A.H., Lutz, T., Baddeley, D., and Soeller, C. (2020). 3D super-resolution microscopy performance and quantitative analysis assessment using DNA-PAINT and DNA origami test samples. Methods *174*, 56–71. https://doi.org/10.1016/j.ymeth.2019.05.018.

41. Scheckenbach, M., Bauer, J., Zähringer, J., Selbach, F., and Tinnefeld, P. (2020). DNA origami nanorulers and emerging reference structures. Apl. Mater. *8*, 110902. https://doi.org/10.1063/5.0022885.

42. Jimenez, A., Friedl, K., and Leterrier, C. (2020). About samples, giving examples: Optimized Single Molecule Localization Microscopy. Methods *174*, 100–114. https://doi.org/10.1016/j.ymeth.2019.05.008.

43. Endesfelder, U., Malkusch, S., Fricke, F., and Heilemann, M. (2014). A simple method to estimate the average localization precision of a single-molecule localization microscopy experiment. Histochem. Cell Biol. *141*, 629–638. https://doi.org/10.1007/s00418-014-1192-3.

44. Xu, K., Zhong, G., and Zhuang, X. (2013). Actin, spectrin, and associated proteins form a periodic cytoskeletal structure in axons. Science *339*, 452–456. https://doi.org/10.1126/science.1232251.

45. Leterrier, C. (2021). Putting the axonal periodic scaffold in order. Curr. Opin. Neurobiol. *69*, 33–40. https://doi.org/10.1016/j.conb.2020.12.015.

46. Cabriel, C., Bourg, N., Jouchet, P., Dupuis, G., Leterrier, C., Baron, A., Badet-Denisot, M.-A., Vauzeilles, B., Fort, E., and Lévêque-Fort, S. (2019). Combining 3D single molecule localization strategies for reproducible bioimaging. Nat. Commun. *10*, 1980. https://doi.org/10.1038/s41467-019-09901-8.

47. Zhong, G., He, J., Zhou, R., Lorenzo, D., Babcock, H.P., Bennett, V., and Zhuang, X. (2014). Developmental mechanism of the periodic membrane skeleton in axons. Elife *3*, e04581. https://doi.org/10.7554/elife.04581.

48. Huang, B., Wang, W., Bates, M., and Zhuang, X. (2008). Three-dimensional super-resolution imaging by stochastic optical reconstruction microscopy. Science *319*, 810–813. https://doi.org/10.1126/science.1153529.

49. Hajj, B., El Beheiry, M., Izeddin, I., Darzacq, X., and Dahan, M. (2014). Accessing the third dimension in localization-based super-resolution microscopy. Phys. Chem. Chem. Phys. *16*, 16340–16348. https://doi.org/10.1039/c4cp01380h.

50. von Diezmann, L., Shechtman, Y., and Moerner, W.E. (2017). Three-Dimensional Localization of Single Molecules for Super-Resolution Imaging and Single-Particle Tracking. Chem. Rev. *117*, 7244–7275. https://doi.org/10.1021/acs.chemrev.6b00629.

51. Früh, S.M., Matti, U., Spycher, P.R., Rubini, M., Lickert, S., Schlichthaerle, T., Jungmann, R., Vogel, V., Ries, J., and Schoen, I. (2021). Site-Specifically-Labeled Antibodies for Super-Resolution Microscopy Reveal In Situ Linkage Errors. ACS Nano *15*, 12161–12170. https://doi.org/10.1021/acsnano.1c03677.

52. Wang, B., Zhao, Z., Xiong, M., Yan, R., and Xu, K. (2022). The endoplasmic reticulum adopts two distinct tubule forms. Proc. Natl. Acad. Sci. USA *119*, e2117559119. https://doi.org/10.1073/pnas.2117559119.

53. Zhou, R., Han, B., Xia, C., and Zhuang, X. (2019). Membrane-associated periodic skeleton is a signaling platform for RTK transactivation in neurons. Science *365*, 929–934. https://doi.org/10.1126/science.aaw5937.

54. Sabinina, V.J., Hossain, M.J., Hériché, J.K., Hoess, P., Nijmeijer, B., Mosalaganti, S., Kueblbeck, M., Callegari, A., Szymborska, A., Beck, M., et al. (2021). Three-dimensional superresolution fluorescence microscopy maps the variable molecular architecture of the nuclear pore complex. Mol. Biol. Cell *32*, 1523–1533. https://doi.org/10.1091/mbc.e20-11-0728.

55. Lampe, A., Tadeus, G., and Schmoranzer, J. (2015). Spectral demixing avoids registration errors and reduces noise in multicolor localization-based super-resolution microscopy. Methods Appl. Fluoresc. *3*, 034006. https://doi.org/10.1088/2050-6120/3/3/034006.

56. Gazzola, M., Schaeffer, A., Butler-Hallissey, C., Friedl, K., Vianay, B., Gaillard, J., Leterrier, C., Blanchoin, L., and Théry, M. (2023). Microtubules

self-repair in living cells. Curr. Biol. *33*, 122–133.e4. https://doi.org/10.1016/j.cub.2022.11.060.

57. Jackson, R.E., Compans, B., and Burrone, J. (2022). Correlative Live-Cell and Super-Resolution Imaging to Link Presynaptic Molecular Organisation With Function. Front. Synaptic Neurosci. *14*, 830583. https://doi.org/10.3389/fnsyn.2022.830583.

58. Tomer, D., Arriagada, C., Munshi, S., Alexander, B.E., French, B., Vedula, P., Caorsi, V., House, A., Guvendiren, M., Kashina, A., et al. (2022). A new mechanism of fibronectin fibril assembly revealed by live imaging and super-resolution microscopy. J. Cell Sci. *135*, jcs260120. https://doi.org/10.1242/jcs.260120.

59. Clowsley, A.H., Kaufhold, W.T., Lutz, T., Meletiou, A., Di Michele, L., and Soeller, C. (2021). Repeat DNA-PAINT suppresses background and non-specific signals in optical nanoscopy. Nat. Commun. *12*, 501. https://doi.org/10.1038/s41467-020-20686-z.

60. Schindelin, J., Arganda-Carreras, I., Frise, E., Kaynig, V., Longair, M., Pietzsch, T., Preibisch, S., Rueden, C., Saalfeld, S., Schmid, B., et al. (2012). Fiji: an open-source platform for biological-image analysis. Nat. Methods *9*, 676–682. https://doi.org/10.1038/nmeth.2019.

61. Ovesný, M., Křížek, P., Borkovec, J., Svindrych, Z., and Hagen, G.M. (2014). ThunderSTORM: a comprehensive ImageJ plug-in for PALM and STORM data analysis and super-resolution imaging. Bioinformatics *30*, 2389–2390. https://doi.org/10.1093/bioinformatics/btu202.

62. Leterrier, C., Potier, J., Caillol, G., Debarnot, C., Rueda Boroni, F., and Dargent, B. (2015). Nanoscale Architecture of the Axon Initial Segment Reveals an Organized and Robust Scaffold. Cell Rep. *13*, 2781–2793. https://doi.org/10.1016/j.celrep.2015.11.051.

63. Virtanen, P., Gommers, R., Oliphant, T.E., Haberland, M., Reddy, T., Cournapeau, D., Burovski, E., Peterson, P., Weckesser, W., Bright, J., et al. (2020). SciPy 1.0: fundamental algorithms for scientific computing in Python. Nat. Methods *17*, 261–272. https://doi.org/10.1038/s41592-019-0686-2.

64. Hunter, J.D. (2007). Matplotlib: A 2D Graphics Environment. Comput. Sci. Eng. *9*, 90–95. https://doi.org/10.1109/mcse.2007.55.

65. Kaech, S., and Banker, G. (2006). Culturing hippocampal neurons. Nat. Protoc. *1*, 2406–2415. https://doi.org/10.1038/nprot.2006.356.

66. Izeddin, I., Boulanger, J., Racine, V., Specht, C.G., Kechkar, A., Nair, D., Triller, A., Choquet, D., Dahan, M., and Sibarita, J.B. (2012). Wavelet analysis for single molecule localization microscopy. Opt Express *20*, 2081–2095. https://doi.org/10.1364/oe.20.002081.

67. Bourg, N., Mayet, C., Dupuis, G., Barroca, T., Bon, P., Lécart, S., Fort, E., and Lévêque-Fort, S. (2015). Direct optical nanoscopy with axially localized detection. Nat. Photonics *9*, 587–593. https://doi.org/10.1038/nphoton.2015.132.

68. Tukey, J.W. (1949). Comparing Individual Means in the Analysis of Variance. Biometrics *5*, 99–114. https://doi.org/10.2307/3001913.

Please cite this article in press as: Friedl et al., Assessing crosstalk in simultaneous multicolor single-molecule localization microscopy, Cell Reports Methods (2023), https://doi.org/10.1016/j.crmeth.2023.100571

STAR★METHODS

KEY RESOURCES TABLE

REAGENT or RESOURCE	SOURCE	IDENTIFIER
Antibodies		
Mouse monoclonal α-tubulin (IgG1, B512)	Sigma	T5168; RRID: AB_477579
Mouse monoclonal α-tubulin (IgG1, DM1A)	Sigma	T6199; RRID: AB_477583
Rabbit polyclonal clathrin hevy-chain	abcam	ab21679; RRID: AB_2083165
Mouse monoclonal β2-spectrin (IgG1, clone 42)	BD biosciences	612563; RRID: AB_399854
Rabbit polyclonal adducin	abcam	ab51130; RRID: AB_867519
Sheep polyclonal RTN4b	Bio-Techne	AF6034; RRID:AB_10573837
Donkey anti mouse F1 docking strand	Massive Photonics	custom
Donkey anti rabbit F2 docking strand	Massive Photonics	custom
Donkey anti mouse Alexa Fluor 647	ThermoFisher	A31571; RRID: AB_162542
Donkey anti rabbit Alexa Fluor 647	Jackson ImmunoResearch	711-605-152; RRID: AB_2492288
Donkey anti mouse CF660C	Biotium	BTM20815-500UL
Donkey anti rabbit CF660C	Biotium	BTM20816-500UL
Donkey anti mouse CF680	Biotium	BTM20819-500UL
Donkey anti rabbit CF680	Biotium	BTM20820-500UL
Goat anti mouse CF680	Biotium	BTM20065
Biological samples		
Cultured hippocampal neurons from E18 rat embryos	Janvier labs	Wistar rat embryos
Critical commercial assays		
Abbelight STORM buffer	Abbelight	N/A
Flow chamber with custom 2-size, 2-color nanorulers	Massive Photonics	N/A
Experimental models: Cell lines		
COS-7 cells	ATCC	ATCC CRL-1651; RRID: CVCL_0224
Software and algorithms		
Fiji	Schindelin et al.[60]	https://fiji.sc/
ThunderSTORM plugin	Ovesny et al.[61]	https://github.com/kjamartens/thunderstorm
ChriSTORM Fiji scripts (reconstruction, splitROIs)	Leterrier et al.[62]	https://github.com/cleterrier/ChriSTORM
Measure ROI Fiji scripts (Profile alignment)	Leterrier et al.[62]	https://github.com/cleterrier/Measure_ROIs
Python version 3.7	Python Software Foundation	https://www.python.org
Scipy	Virtanen et al.[63]	https://scipy.org/
Matplotlib	Hunter et al.[64]	https://matplotlib.org/
Python scripts for crosstalk analysis, Figures 1,2, and 6	This Paper	https://zenodo.org/record/8010746
Python script for statistical analysis, Figures 3 and 4	This Paper	https://zenodo.org/record/8010746
Python script for calculating NeNa values	This Paper	https://zenodo.org/record/8010746
Python script for structure "hollowness", Figure S7	This Paper	https://zenodo.org/record/8010746
Abbelight NeoLive Imaging	Abbelight	https://abbelight.com
Abbelight NeoAnalysis	Abbelight	https://abbelight.com

Please cite this article in press as: Friedl et al., Assessing crosstalk in simultaneous multicolor single-molecule localization microscopy, Cell Reports Methods (2023), https://doi.org/10.1016/j.crmeth.2023.100571

RESOURCE AVAILABILITY

Lead contact

Further information and requests for resources and reagents should be directed to and will be fulfilled by the lead contact, Christophe Leterrier (christophe.leterrier@univ-amu.fr).

Materials availability

This study did not generate new unique reagents.

Data and code availability

Microscopy data reported in this paper will be shared by the lead contact upon request. Original code has been deposited at Zenodo and is publicly available as of the date of publication (see key resources table). Postprocessing of localization data was done with *Neo* Analysis software (Abbelight). Additional software used for rendering of images, quantification of crosstalk, alignment of profiles and FWHM calculation can be found in the relevant GitHub repositories (https://github.com/cleterrier?tab=repositories). Additional information required to reanalyze the data reported in this paper is available from the lead contact upon request.

EXPERIMENTAL MODEL AND STUDY PARTICIPANT DETAILS

COS-7 cell culture

COS-7 cells (ATCC CRL-1651, isolated from a male Green African monkey) were cultured at 37°C with 5% CO_2 in DMEM medium (ThermoFisher #61965026), supplemented with fetal bovine serum (ThermoFisher, #A3381901) and antibiotics (Penicillin/Streptomycin, ThermoFisher #15140122). 24 h after seeding on poly-L-lysine (Sigma #P2636) coated coverslips (#1.5H 18 mm Marienfeld, VWR) to a density of about 10%, they were fixed and prepared for microscopy observations.

Neuron culture

All procedures involving animal cell culture followed the guidelines from European Animal Care and Use Committee (86/609/CEE) and were approved by the Aix-Marseille Université ethics committee (agreement D13-055-8). Rat hippocampal neurons were cultured at 37°C with 5% CO_2 on top of a glia feeder layer according to the Banker protocol.[65] Briefly, hippocampi from Wistar rat embryos of both sexes (Janvier Labs) were dissected, then cells were homogenized and seeded on poly-L-lysine coated #1.5H glass coverslips to a density of 4000 cells per cm^2 in MEM (ThermoFisher #21090-055) supplemented with fetal bovine serum, which was replaced after 3 h with Neurobasal medium (ThermoFisher #21103-049) supplemented with B27 (Thermo Fisher #17504-044). Mature neurons were fixed after 14 days in culture.

METHOD DETAILS

COS-7 fixation

COS-7 were either extracted and fixed with a two-step protocol using glutaraldehyde as a fixative (Sigma #3G5882) or fixed in a single step with a mixture of glutaraldehyde and paraformaldehyde (PFA, Delta Microscopy #EM-15714). For the two-step extraction/fixation with glutaraldehyde (tubulin/clathrin staining), cells were first extracted by a 45-s incubation with 37°C pre-heated 0.1% glutaraldehyde, 0.25% Triton (Sigma #T8787) in PEM buffer (80mM PIPES, 2mM MgCl2, 5mM EGTA, pH 6.8) then fixed for 10 min at 37°C in pre-heated 2% glutaraldehyde, 0.5% Triton in PEM. For the single step glutaraldehyde/PFA fixation (tubulin/clathrin/rtn4b staining), cells were fixed for 10 min at 37°C with 0.1% glutaraldehyde, 4%PFA, and 4% (w/v) sucrose in PEM buffer. Following both fixation procedures, cells were rinsed in phosphate buffer (PB, 0.1 M pH 7.3), then residual glutaraldehyde was quenched for 7 min using 10 mg/mL sodium borohydride (Sigma #213462) in PB before further rinses with PB.[42]

Neuronal fixation

Mature neurons were fixed after 14 days in culture using 4% PFA and 4% sucrose in PEM buffer for 10 min at room temperature (RT) and rinsed with PB.

Immunostaining and antibodies

Blocking and permeabilization were performed in immunocytochemistry buffer (ICC: 0.22% gelatin, 0.1% Triton X-100 in PB) for 1 to 3 h on a rocking table. Cells were incubated overnight at 4°C with primary antibodies diluted in ICC, rinsed, and incubated with secondary antibodies diluted in ICC for 1 h at RT. After final rinses in ICC and PB, the samples were stored in PB with 0.02% (v/v) sodium azide (Sigma #08591) before imaging.

SMLM microscope

The SMLM microscope used for all imaging is based on either an Olympus IX81 inverted microscope stand equipped with a focus stabilization system (ZDC2, Olympus) and a 100X, NA 1.49 oil objective (APON100XHOTIRF, Olympus) or a Nikon Ti2 inverted

microscope stand equipped with a motorized stage, a piezo Z-stage (Mad City Labs), a focus stabilization system (Perfect Focus System, Nikon) and a 100X, NA 1.49 oil objective (CFI SR HP Apochromat TIRF 100XC, Nikon). An Abbelight SAFe360 module is attached to the side C-mount of the stand. It receives laser excitation from an Oxxius L4Cc Combiner equipped with 640 nm (500 mW), 532 nm (400 mW), 488 nm (150 mW) and 405 nm (100 mW) lasers through the ASTER scanning module (Abbelight).[37] Separation between excitation and emission bands is done using a quad-band dichroic mirror (Semrock, Di03-R405/488/532/635-t3-25x36), and emission light is further separated using a dichroic mirror (662 nm Semrock FF662-FDi02-t3-25x36 or 700 nm FF699-FDi01-t3-25x36), filtered on both paths by quad-band emission filters (Semrock FF01-446/510/581/703-25) and captured by two Hamamatsu Photonics Flash4 V3 sCMOS cameras. For 3D imaging, the point spread functions were shaped using two cylindrical lenses inserted in the optical pathway between the second dichroic mirror and the cameras.

DNA-PAINT acquisition

For DNA-PAINT imaging, samples were mounted in an open metal chamber (Ludin Chamber, Life Imaging Services) allowing for easy medium exchange. The "regular" imager strands (I1 and I3)[9] or repetitive-sequence "fastPaint" imager strands (IF1 and IF2)[13] were diluted in imaging buffer and washed off with washing buffer (imager strands and buffers from Massive Photonics). Fluorescence illumination was performed using the 532 nm and 640 nm lasers in Highly Inclined and Laminated Optical sheet (HILO) illumination to restrict illumination to ~1 μm above the coverslip for minimal background fluorescence from unbound imagers. The illumination strength was adapted to the field of view we chose, between 50 μm × 50 μm and 80 μm × 80 μm. With using 40–100% of the laser, the irradiance resulted in 0.55–3.44 kW/cm^2. The emission was split in a reflected and a transmitted pathway by a 662 nm dichroic mirror (Semrock, FF662-FDi02-t3-25x36); acquisitions were acquired with exposure times between 30 and 100 ms. A detailed table of the parameters for each acquisition is provided in Table S1.

Spectral demixing-STORM acquisition

dSTORM samples were mounted in sealed silicone chambers filled with Abbelight STORM buffer kit. The samples were labeled with secondary antibodies conjugated with AF647 and CF680 for two-target spectral demixing; for three targets a staining with an antibody conjugated with CF660C was added (see "key resources table"). Illumination was performed using the 640 nm laser (Between 1.23 and 13.62 kW/cm^2 depending on the field of view) with manual increase of low-power illumination using the 405 nm laser line aid fluorophore recovery from long-lived dark states. HiLO illumination was used to restrict illumination to ~1 μm above the coverslip. The detection pathway was split into a reflected and a transmitted part by a 700 nm dichroic mirror (Semrock, FF699-Fdi01-t3-25x36). Exposure time was chosen depending on the size of the field of view between 5 ms (30 μm μm x 30 μm field of view) and 50 ms (100 μm × 100 μm field of view); and between 15,000 and 60,000 frames were acquired. All parameters per acquisition are summarized in Table S1.

Nanorulers sample and imaging

The DNA origami-based nanorulers slide was custom ordered (Gattaquant) and contains two types of 3-spots nanorulers deposited in a single fluidic cavity allowing for medium exchange and rinses. One nanoruler type has spots spaced by 40 nm tagged with a P1 docking strand, the other one has spots spaced by 80 nm tagged with a P3 docking strand. For simultaneous 2-color DNA-PAINT, imager strands conjugated with Cy3B and Atto655 (all imagers from Massive Photonics) were diluted in phosphate buffer saline (PBS) + 10 mM $MgCl_2$ to a concentration between 500 p.m. and 20 nM. The sample was simultaneously illuminated in HiLO with 532 nm (0.37–0.71 kW/cm^2) and 640 nm (0.91–1.77 kW/cm^2) lasers, emission was split using the 662 nm dichroic mirror and recorded 60,000 frames with an exposure time of 50 ms on the two cameras on a 70 μm × 70 μm field of view.

For far-red spectral demixing DNA-PAINT, 3 to 10 nM I1-Atto680 and 2 nM I3-Atto655 were used to reveal the nanorulers in PBS +10 mM $MgCl_2$; the sample was illuminated with a single 640 nm laser (2.5 kW/cm^2) in HiLO and emission was split with the 700 nm dichroic mirror. The cameras were set to an exposure time of 100 ms and to record 60,000 frames.

SMLM data processing

Acquired PAINT and STORM sequences were processed using the Abbelight *Neo* Analysis software. Detection of intensity peaks used a wavelet algorithm[66] after local means background estimation and removal. Intensity peaks at least twice as high as the background with a size of 3x3 to 7x7 pixels area (300–700 nm) were considered a single-molecule blinking event and further processed for fitting using Gaussian fitting with least-squares error. The number of photons emitted by the blinking event was estimated from the background-subtracted raw data by integration over a 11x11 pixel round area (1.1 μm diameter).[67] Frame sequences from each camera were processed individually to generate two lists of localizations containing their coordinates and photon number. Three-dimensional astigmatism-based acquisition were fitted for Z position according to the eccentricity of the PSF using a calibration obtained on 100 nm beads.

Channel assignment (demixing) from two-camera data

After fitting, two images were reconstructed using the localizations list from each camera and were then aligned using an affine transform to correct for lateral aberrations (OpenCV, "Motion_affine", correction for rotation, translation, scale and shear). The correction is illustrated in Figure S5. The localization coordinates obtained from each camera image sequence were then modified using the

determined affine transformation, before checking for pairs of localizations between the two cameras: localizations appearing at the same coordinates with a tolerance of 500 nm on identical frames. For each detected pair, the ratio of the emitted photons was calculated with:

R = I(*trans*)/I(*trans*) + I(*refl*)

where I(*trans*) is the number of photons for the localization on the transmitted path camera image, and I(refl) the number of photons for the localization on the reflected path camera image. Unpaired localizations only appearing on the reflected or transmitted path camera image were assigned a ratio of 0 or 1, respectively. For S2C-DNA-PAINT data, channels were either directly defined from the localization files from each camera, or after demixing. In the latter case, localizations with ratios 0–0.01 were assigned to the Cy3B/Atto565 channel, and localizations with rations 0.99–1 were assigned to the Atto643 channel. For 2-color SD-dSTORM data, localizations with ratios 0–0.29 were assigned to the AF647 channel, and those with ratios 0.5–1 were assigned to the CF680 channel. For 3-color SD-dSTORM data, localizations with ratios 0.01–0.29 were assigned to the AF647 channel, 0.31–0.45 to the CF660C channel, 0.5–0.99 to the CF680 channel. After demixing, separate localization files were generated for each channel, with the final coordinate of each localization determined using weighted averages of the localization precision of the localizations on the two cameras and these localization files were used to reconstruct images for each channel.

QUANTIFICATION AND STATISTICAL ANALYSIS

Crosstalk analysis

Analysis of crosstalk from nanorulers images

from each acquisition, on each channel, >19 nanorulers were selected (39–46 total per channel for S2C-DNA-PAINT and 70 total per channel for SD-dSTORM) by hand to ensure selection of intact nanorulers. A ROI was drawn around the selected Nanorulers and the ROI applied on both channels. The included localizations were counted using a dedicated macro ("Split Locs by ROI" macro available from the ChriSTORM GitHub repository at https://github.com/cleterrier/ChriSTORM/) in Fiji software.[60] The number of localizations found in the ROI in the non-target channel (i.e., localizations found in the longer wavelength channel, in a ROI drawn around a nanoruler in the shorter wavelength channel), were divided by the total of localizations found in the same ROI on both channels to calculate the crosstalk. A python script was created to calculate mean and SEM (Scipy)[63] and render plots (Matplotlib).[64]

Analysis of multicolor DNA-PAINT crosstalk from single-target samples

DNA-PAINT crosstalk was evaluated using a two-step strategy with varying imagers (Figure S3). A sample labeled for a single target and docking strand (example: microtubules with an F2-coupled secondary antibody) was first imaged with two non-target imagers (A1Ch1_NT: IF1-Atto565 and A1Ch2_NT: IF1-Atto643). After rinses, the same field of view was then imaged using a target and a non-target imager (A2Ch1_T: IF2-Atto565 and A2Ch2_NT: IF1-Atto643). Both acquisition sequences (A1 and A2) were processed using localization and optional demixing. Images for all channels from both acquisition sequences were reconstructed using the histogram method in the Fiji plugin ThunderSTORM,[61] where each pixel (15 nm in size) takes a value corresponding to the number of localizations inside this pixel. A ROI for the target (microtubules) was obtained by thresholding the reconstructed image of the target imager from the second acquisition sequence (A2Ch1_T: IF2-Atto565) and used to measure the number of localizations in this channel (A2Ch2_T), then in all other channels from both acquisition sequences (A1Ch1_NT, A1Ch2_NT and A2Ch2_NT). The crosstalk of the target channel (Ch1: Atto565) into the non-target channel (Ch2: Atto643) is then defined as the number of localizations in the non-target channel (Ch2: Atto643) that are added by the presence of a target imager in the target channel (Ch1: Atto565), corrected for the background obtained using non-target imagers in each channel (A1Ch2_NT and A1Ch1_NT), expressed in percentage:

Crosstalk (Ch1/Atto565 into Ch2/Atto643) = (A2Ch2_NT – A1Ch2_NT)/(A2Ch1_T – A1Ch1_NT).

Analysis of demixing-STORM crosstalk from single-target samples

sample were labeled for a single target (microtubules) with a given fluorophore, then imaged and processed according to the demixing-STORM procedure above. Localizations were then assigned to two (AF647 and CF680) or three (AF647, CF660C, CF680) channels using the demixing procedure detailed above, and the images from each channel were reconstructed using the histogram method. A ROI was obtained by thresholding the microtubules on the channel corresponding to the fluorophore used (target channel), and the number of localizations was measured inside this ROI on the images of the target channel and those of the non-target channel(s) using the "Split Locs by ROI" macro. The proportion of localizations within the ROI in each channel - which is the crosstalk value for non-target channels - was obtained by dividing the number of localizations in this channel by the total number of localizations in all channels and was expressed as a percentage.

Analysis of multicolor DNA-PAINT and demixing-STORM crosstalk from multicolor samples

a similar procedure was used to estimate crosstalk on samples labeled for multiple targets. After imaging, processing and demixing into channels, ROIs were obtained for each channel by thresholding the corresponding reconstructed images. To avoid bias from target overlap (such as clathrin-coated pit overlapping with a microtubule), overlapping areas of ROIs from the different channels were excluded before counting the localizations within each ROI on the target and non-target images. The localization proportions (crosstalk value for non-target images) were then calculated as above.

Please cite this article in press as: Friedl et al., Assessing crosstalk in simultaneous multicolor single-molecule localization microscopy, Cell Reports Methods (2023), https://doi.org/10.1016/j.crmeth.2023.100571

Analysis of the actin/spectrin periodicity along axons

The investigation of the effect of crosstalk at different labeling densities was performed on neurons labeled for β2-spectrin and adducin, which form a complementary periodic scaffold with a 190 nm periodicity. After S2C-DNA-PAINT or SD-dSTORM imaging of the samples, the acquisition sequences were processed and demixed into two channels as described above. Linear segments of axons were manually selected and analyzed by autocorrelation for each channel using a custom script ("Autocorrelation" script available at the Process_Profile GitHub repository https://github.com/cleterrier/Process_Profiles), to determine if the presence of the periodicity observed in one channel could be perturbed by crosstalk from the presence of a second channel. All segments were analyzed independently to keep the analysis consistent between S2C-DNA-PAINT and SD-dSTORM. This was done by subtracting the amplitude of the autocorrelation curve at the first valley (95 nm shift for a 15-nm pixel size) to its amplitude at the first peak (195 nm shift). The statistical analysis was performed pairwise with a Tukey-Cramer post-hoc comparison[68] based on a script by Renesh Bedre (https://www.reneshbedre.com/blog/anova.html, using the modules statsmodel, scipy, and bioinfokit). Code is available on Zenodo (see Key resources table).

Microtubule cross-section analysis

Microtubules from 3D acquisitions with S2C-DNA-PAINT and SD-dSTORM were analyzed for Full Width at Half Maximum (FWHM) in the X and Z dimension. Three microtubule sections were taken from each image and turned into perpendicular XZ cross-sections reconstructed with 4-nm pixel size ("Line ROIs to Slices" and "Generate Zooms and Slices" macros form the ChriSTORM GitHub repository).[62] The intensity profile was taken from the whole width of the reconstructions and aligned ("ProFeatFit" script available from the Process_Profile GitHub repository at https://github.com/cleterrier/Process_Profiles).[62] The profiles were then averaged and fitted with a Gaussian distribution and the FWHM calculated using scipy optimize functions.

Microtubule and endoplasmic reticulum 2D profile analysis

Ten microtubule sections from 2D acquisitions with S2C-DNA-PAINT and SD-dSTORM were analyzed for Full Width at Half Maximum (FWHM) in the X and Z dimension. For the ER, five areas of visible hollowness were analyzed. Profiles were normalized and centered to form a mean profile where hollowness is measured as the distance between the two peaks. Additionally, six regions of the ER with a single-wall visible were analyzed to determine their width. The python scripts available at Zenodo (see key resources table).

Estimation of localization precision with NeNa

Estimation of localization precision was made using a custom python script (version 3.10.9) based on Endesfelder et al.[43] Code is available at Zenodo (see "key resources table"). Briefly, molecules detected on consecutive frames are identified and their distances are measured. The distribution of lateral distance between molecules is the $I_{rayleigh}$ distribution, which is fitted with scipy's leastsq function. To correct for false positives, an additional Gaussian and slope curves are included in the fitting model.

Cell Reports Methods, Volume *3*

Supplemental information

Assessing crosstalk in simultaneous multicolor single-molecule localization microscopy

Karoline Friedl, Adrien Mau, Fanny Boroni-Rueda, Valentina Caorsi, Nicolas Bourg, Sandrine Lévêque-Fort, and Christophe Leterrier

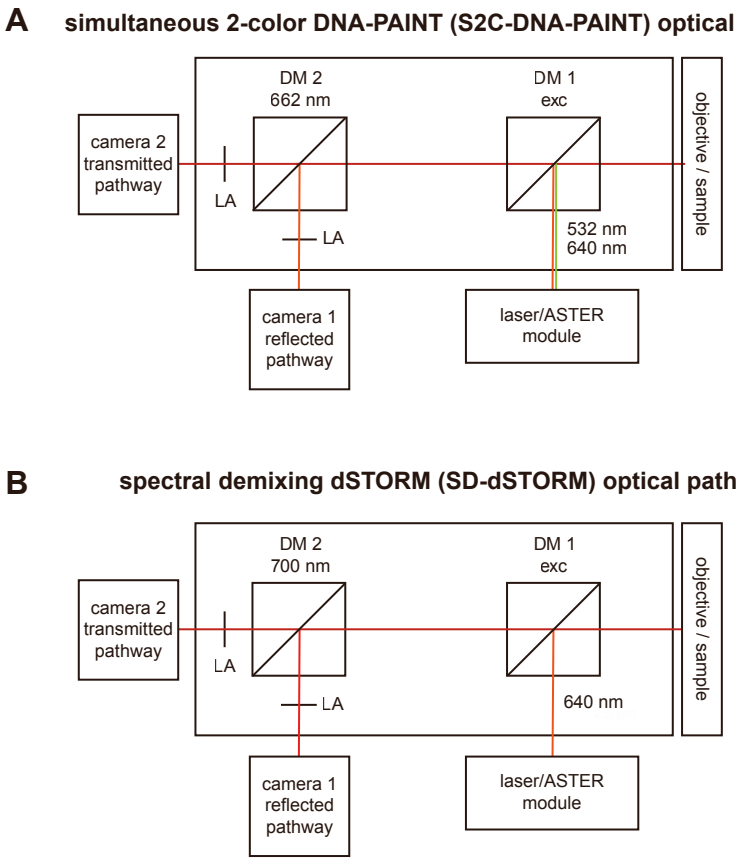

Figure S1. Optical paths for S2C-DNA-PAINT and SD-dSTORM (related to Figures 1 and 2)
(A) Optical path for S2C-DNA-PAINT: the 532 and 640 nm excitation laser beams are reflected by the dichroic mirror DM1 into the microscope body (objective and sample). The fluorescence emitted from the sample travels through DM1, and is split by the 662 nm dichroic mirror DM2 toward the two cameras. For 3D acquisitions, cylindrical lenses (LA) are inserted in front of each camera.
(B) Optical path for SD-dSTORM: the single 640 nm excitation laser beams is reflected by the dichroic mirror DM1 into the microscope body (objective and sample). The fluorescence emitted from the sample travels through DM1, and is split by the 700 nm dichroic mirror DM2 toward the two cameras. For 3D acquisitions, cylindrical lenses (LA) are inserted in front of each camera.

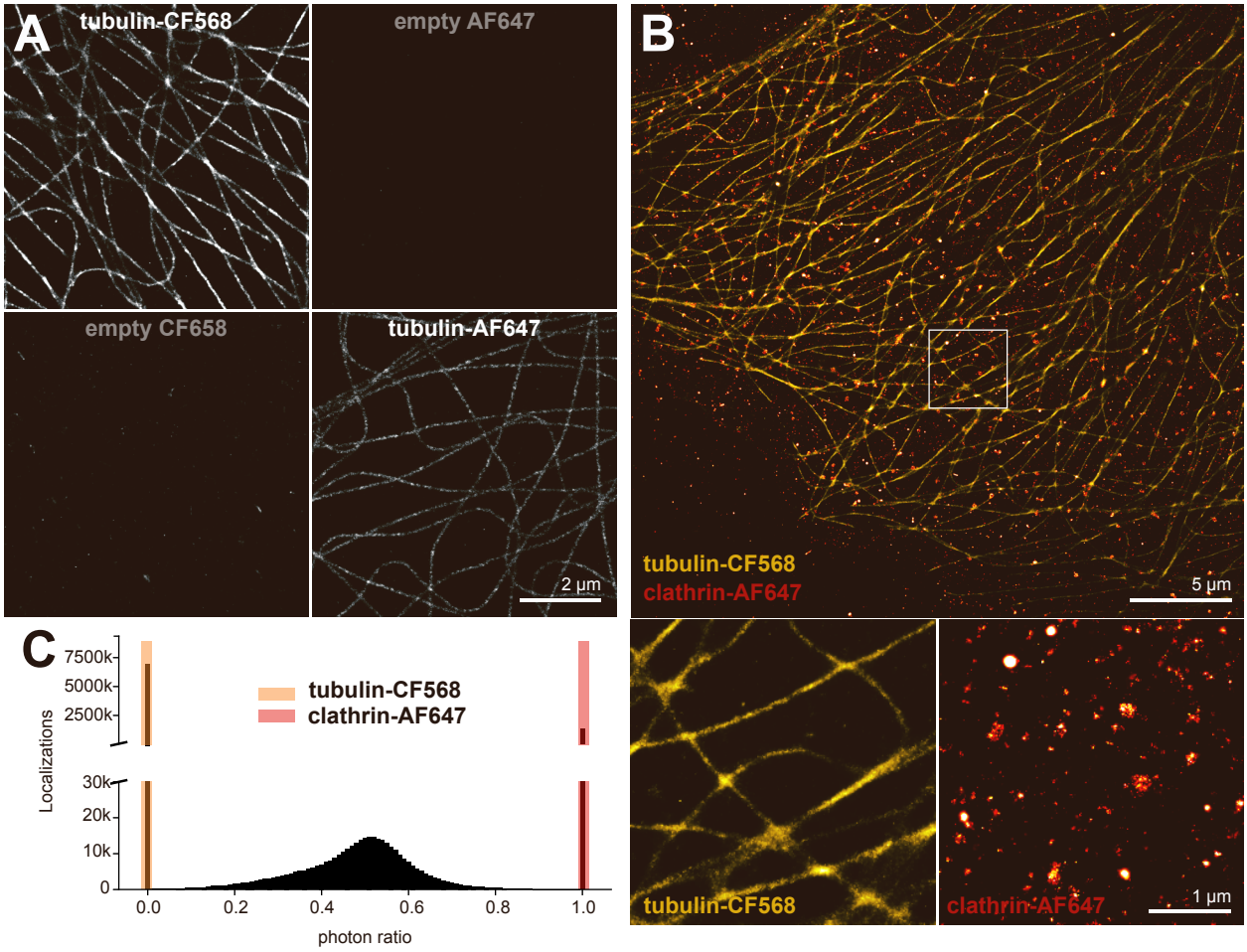

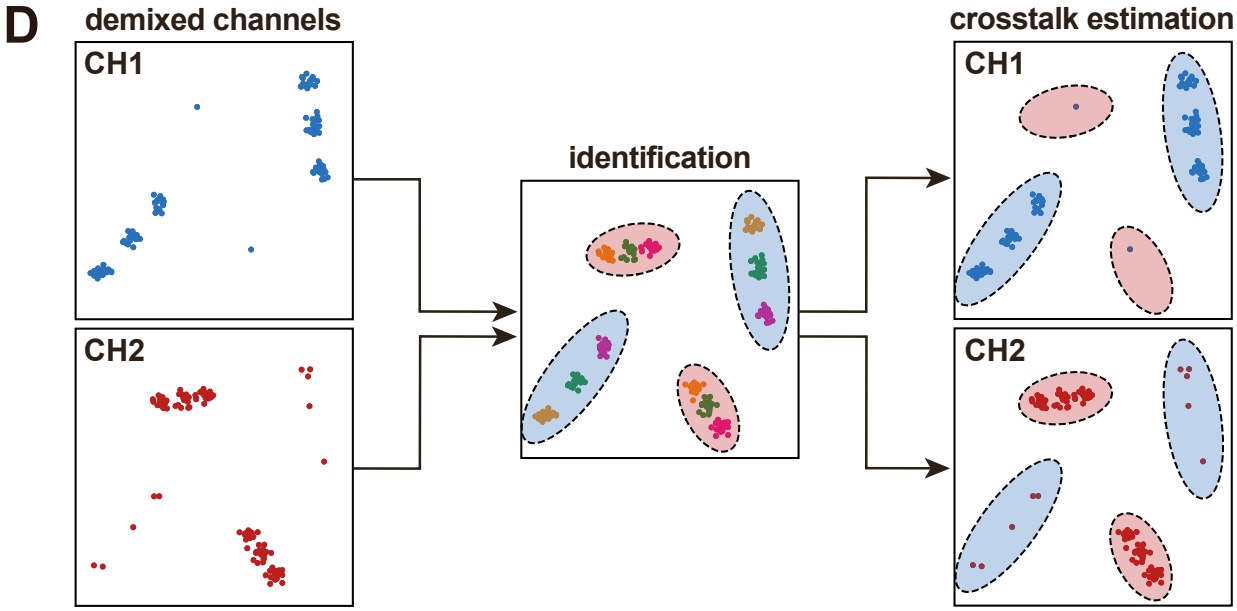

Figure S2. Simultaneous 2-color STORM with CF568 and AF647 and crosstalk analysis with nanorulers (related to Figure 1)
(A) COS cells stained for tubulin with a secondary antibody conjugated to CF568 (top row) or AF647 (bottom row), demixed into 2 channels with the 2-color ratio ranges (0-0.01 for CF568, 0.99-1 for AF647).
(B) Simultaneous 2-color STORM image of a COS cells stained for tubulin with a secondary antibody conjugated to CF568 (orange) and clathrin with a secondary antibody conjugated to AF647 (red), demixed into 2 channels with the 2-color ratio range (0-0.01 for CF568, 0.99-1 for AF647) defined in C. Bottom images are zoomed isolated channels. One can see the low quality of the microtubule image, due to the sub-optimal blinking properties of CF568.
(C) Ratiometric analysis for the image shown in B, with used 2-color ratio ranges highlighted in colors.
(D) Crosstalk analysis with nanorulers: two channels are obtained after acquisition and demixing with pre-determined ratio ranges (left panels). Images were then reviewed and intact, isolated nanorulers were manually selected (>19 per image and channel, center panel, dashed ellipses), distinguished by fluorophore assignment and size. Segmentation ROIs were used on both channels to count the number of localizations and calculate the crosstalk per nanoruler type (right panel; short nanoruler: red ellipses; long nanoruler: blue ellipses).

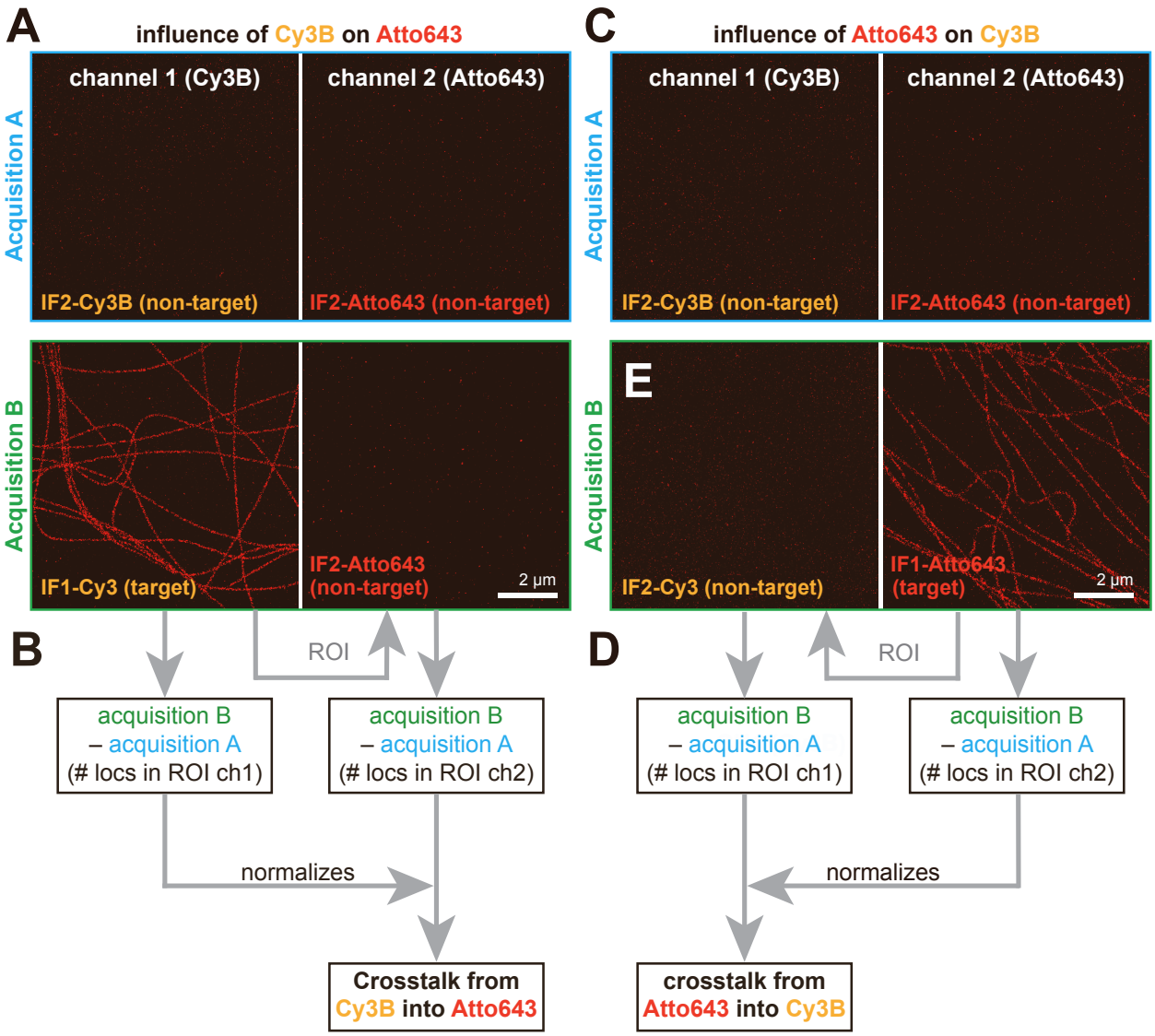

Figure S3. Crosstalk evaluation from single-target staining in S2C-DNA-PAINT based on successive acquisition of background and target images (related to Figure 1)

A-B. Evaluation of the crosstalk from Cy3B (orange) into Atto643 (red): influence of the Cy3B channel signal on the Atto643 signal.
(A) COS-7 cell stained for tubulin with a secondary antibody conjugated to an F1 docking strand is subjected to 2 successive acquisitions: in acquisition A, both channels contain a non-target imager (IF2-Cy3B and IF2-Atto643), resulting in background in both channels (first row, blue). In acquisition B, the Cy3B channel contains a target imager (IF1-Cy3B) resulting in signal, while the Atto643 channel contains a non-target imager (IF2-Atto643), resulting in background (green, bottom row).
(B) A ROI is drawn from segmenting the microtubule signal in the I1-Cy3B channel of acquisition B, and used to measure the number of localizations in all channels. Acquisition A is used to subtract background in both channels from acquisition B, and the remaining localizations in the Atto643 channel in acquisition B (assumed to be due to the presence of Cy3B signal) are normalized by the number of localizations in the Cy3B signal channel of acquisition B, resulting in the crosstalk value for Cy3B into Atto643.
C-D. Evaluation of the crosstalk from Atto643 (red) into Cy3B (orange): influence of the Atto643 channel on the Cy3B signal.
(C) COS-7 cell stained for tubulin with a secondary antibody conjugated to an F1 docking strand is subjected to 2 successive acquisitions: in acquisition A, both channels contain a non-target imager (IF2-Cy3B and IF2-Atto643), resulting in background in both channels (first row, blue). In acquisition B, the Cy3B channel contains a non-target imager (IF2-Cy3B) resulting in background, while the Atto643 channel contains a target imager (IF1-Atto643), resulting in signal (green, bottom row).
(D) A ROI is drawn from segmenting the microtubule signal in the I1-Atto643 channel of acquisition B, and used to measure the number of localizations in all channels. Acquisition A is used to subtract background in both channels from acquisition B, and the remaining localizations in the Cy3B channel in acquisition B (assumed to be due to the presence of Atto643 signal) are normalized by the number of localizations in the Atto643 signal channel of acquisition B, resulting in the crosstalk value for Atto643 into Cy3B.

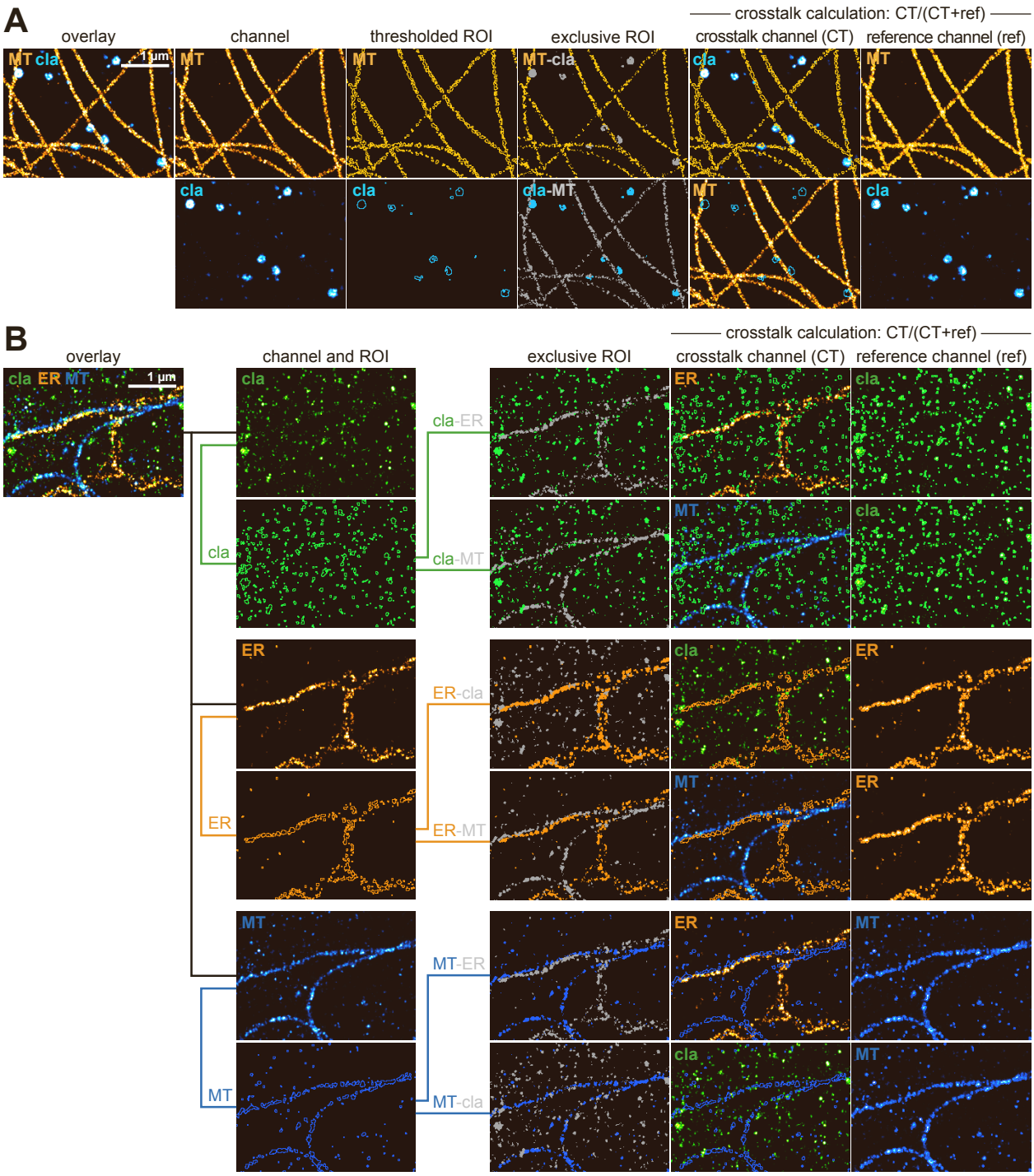

Figure S4. Exclusive ROIs crosstalk measurement on multi-target images (related to Figures 1,2 and 6)
(A) Exclusive ROI crosstalk measurement procedure for a 2-color image of a COS-7 cell stained for microtubules (orange) and clathrin (cyan). From each channel (second column), ROIs are defined by thresholding (third column). Subtraction of each ROI by the other results in exclusive ROIs for each channel (fourth column), that are applied to the crosstalk channel (CT, non-target, fifth column) and to the reference channel (target, sixth column) to calculate the crosstalk value from the number of localizations inside the exclusive ROI in each channel.
(B) Exclusive ROI crosstalk measurement procedure for a 3-color image of a COS-7 cell stained for clathrin (green), ER (orange) and microtubules (cyan). From each channel (second column, top images), ROIs are defined by thresholding (second column, bottom images). Subtraction of each ROI by the others results in two exclusive ROIs for each channel (third column), that are applied to their respective crosstalk channel (CT, non-target, fourth column) and to the reference channel (target, fifth column) to calculate the crosstalk value from the number of localizations inside the exclusive ROI in each channel.

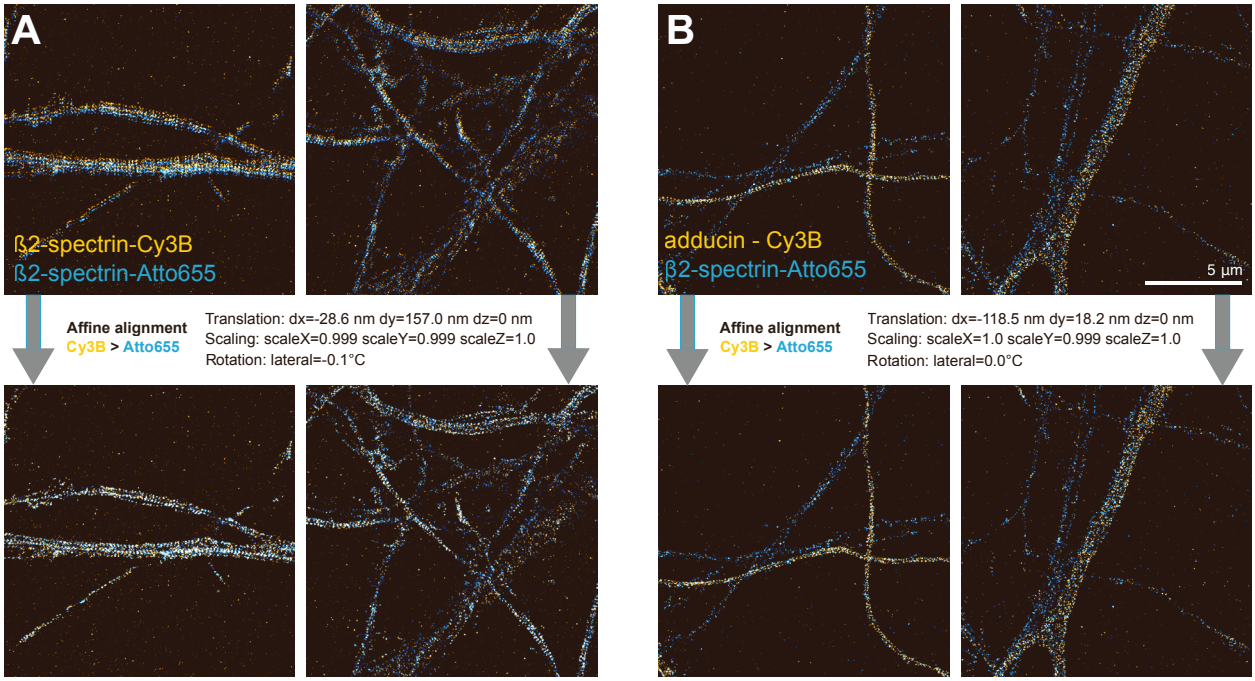

Figure S5. Chromatic aberration correction by channel alignment in S2C-DNA-PAINT (related to Figure 3)
(A) Images from axons of hippocampal neurons stained for β2-spectrin and imaged by S2C-DNA-PAINT in both channels simultaneously using F1-Cy3B (blue) and F1-Atto655 (yellow) before (upper panels) and after (lower panel) correction by affine alignment of the reflected channel (Cy3B) on the transmitted channel (Atto655).
(B) Images from axons of hippocampal neurons stained for adducin (F2-Cy3B imager, yellow) and β2-spectrin (F1-Cy3B imager, blue) imaged by S2C-DNA-PAINT before (upper panels) and after (lower panel) correction by affine alignment of the reflected channel (Cy3B) on the transmitted channel (Atto655).

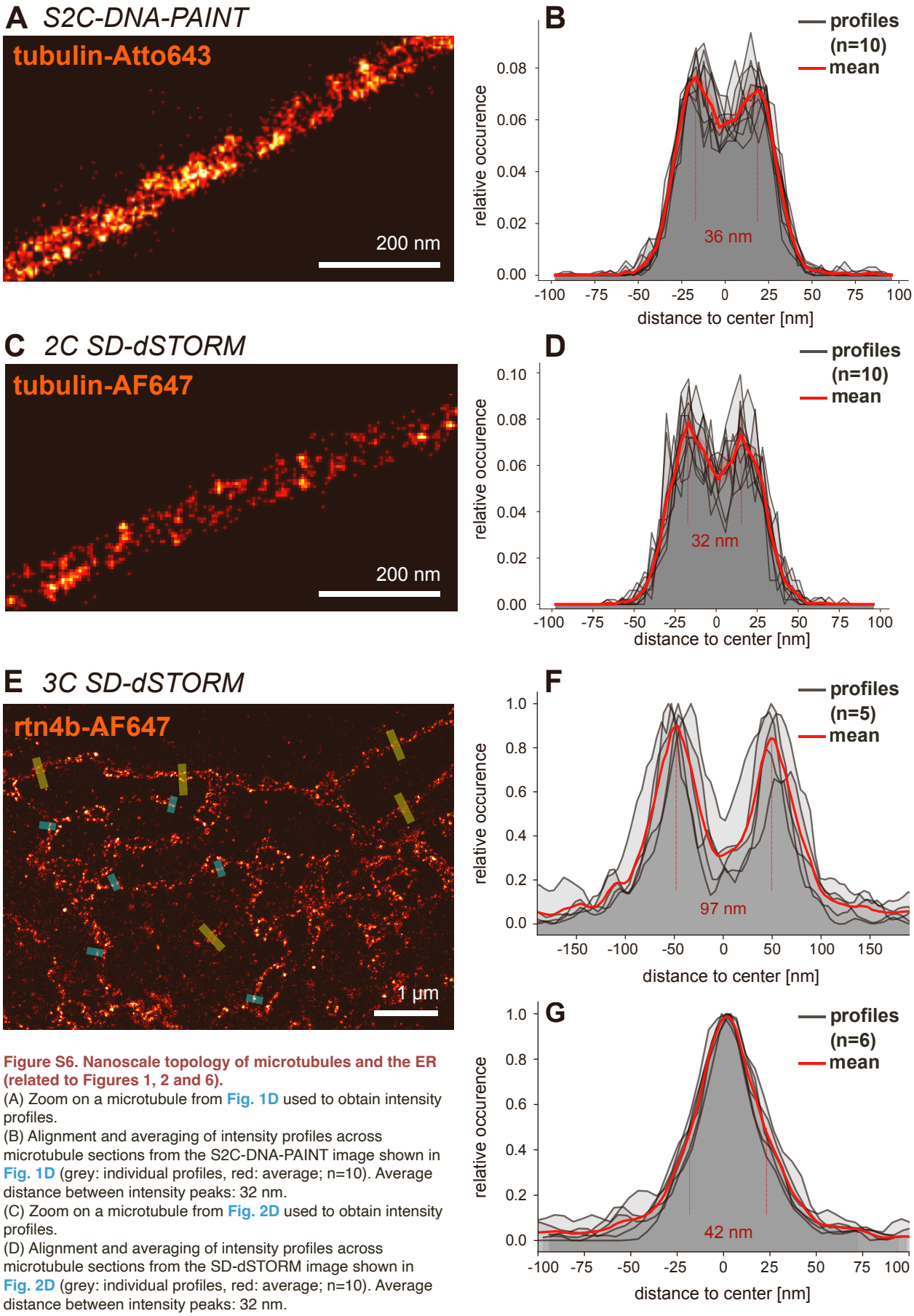

Figure S6. Nanoscale topology of microtubules and the ER (related to Figures 1, 2 and 6).

(A) Zoom on a microtubule from Fig. 1D used to obtain intensity profiles.

(B) Alignment and averaging of intensity profiles across microtubule sections from the S2C-DNA-PAINT image shown in Fig. 1D (grey: individual profiles, red: average; n=10). Average distance between intensity peaks: 32 nm.

(C) Zoom on a microtubule from Fig. 2D used to obtain intensity profiles.

(D) Alignment and averaging of intensity profiles across microtubule sections from the SD-dSTORM image shown in Fig. 2D (grey: individual profiles, red: average; n=10). Average distance between intensity peaks: 32 nm.

(E) Zoom on the ER staining (anti-rtn4b antibody) acquired with three-color SD-dSTORM (Fig. 6D), showing the cross-sections analyzed in E and G (respectively in yellow and cyan).

(F) Alignment and averaging of intensity profiles across hollow tubular sites of the ER, acquired with three-color SD-dSTORM shown in Fig. 6D (grey, individual profiles, red: average; n=5). Average distance between intensity peaks: 97 nm. G. Alignment and averaging of intensity profiles across single ER walls, acquired with three-color SD-dSTORM shown in Fig. 6D (grey, individual profiles, red: average; n=6). Average distance between intensity peaks: 97 nm.

Table S1: Imaging conditions (related to all Figures and Supplementary Figures)

Figure panel	Imaging mode	Target 1	Mean photon number	Target 2	Mean photon number	Target 3	Mean photon number	NeNa (nm)
Fig. 1B	S2C-DNA-PAINT	40 nm-P1 2 nM I1-Cy3B	6399	80 nm-P3 20 nM I3-Atto655	4386			
Fig. 1B	S2C-DNA-PAINT	80 nm-P3 1 2 nM IP3-Cy3B	7104	40 nm-P1 10 nM IP1-Atto655	6587			W1: 25.7 W2: 12.2
Fig. 1C	S2C-DNA-PAINT	tubulin-F1 500 pM IF2-Cy3B	1664	tubulin-F1 1 nM IF2-Atto643	3448			
Fig. 1C	S2C-DNA-PAINT	tubulin-F1 500 pM IF1-Cy3B	3578	tubulin F1 1 nM IF2-Atto643	3127			
Fig. 1C	S2C-DNA-PAINT	tubulin-F1 500 pM IF2-Cy3B	1364	tubulin-F1 1 nM IF1-Atto643	3798			
Fig. 1 A,D	S2C-DNA-PAINT	tubulin-F1 500 pM IF1-Atto643	7424	clathrin-F2 300 pM IF2-Atto565	12166			W1: 14.4 W2: 15.4
Fig. 2B	SD-DNA-PAINT	80 nm-P3 2-10 nM IP3-Atto655	10471	40 nm-P1 10-30 nM IP1-Atto680	10558			W1: 20.2 W2: 21.7
Fig. 2C	SD-dSTORM	tubulin-AF647	5234				697	
Fig. 2C	SD-dSTORM		1829			tubulin-CF680	2316	
Fig. 2 A,D	SD-dSTORM	tubulin-AF647	6171	clathrin-CF680	1291			W1: 15.1 W2: 25.5
Fig. 3	S2C-DNA-PAINT	ß2-spectrin-F1 5-500 pM IF1-Cy3	2128	adducin-F2 6.25-625 pM IF2-Atto643	3606			
Fig. 4	SD-dSTORM	adducin-AF647 (3.3-100%)	8018	ß2-spectrin-CF680 (3.3-100%)	5200			
Fig. 5 A,B,C	S2C-DNA-PAINT	tubulin F1 IF1-Cy3B	3418	clathrin F2 IF2-Atto643	3024			W1: 31.3 W2: 19.7
Fig. 5 D,E,F	SD-dSTORM	tubulin-AF647	4935	clathrin-CF680	2159			W1: 18.8 W2: 23.6
Fig. 6 A,C,F	SD-dSTORM	tubulin-AF647	4664		1277		872	
Fig. 6 A,C,F	SD-dSTORM		2589	tubulin-CF660C	3313		1112	
Fig. 6 A,C,F	SD-dSTORM		1829		1467	tubulin-CF680	2316	
Fig. 6D	SD-dSTORM	RTN4b-AF647	10513	clathrin-CF660C	7547	tubulin-CF680	8740	W1: 24.4 W2: 21.2 W3: 25.8
Fig.S2B	S2C-dSTORM	tubulin-CF568	2613	clathrin-AF647	3627			
Fig.S2A	S2C-dSTORM	tubulin-CF568	2407		2938			
Fig.S2A	S2C-dSTORM		1651	tubulin-AF647	5026			

Figure panel	Imaging mode	Buffer*	Frames	Exposure time (ms)	Acquisition duration (min)	532 nm power (kW/cm^2)	640 nm power (kW/cm^2)	FoV side (µm)	Dichroic mirror	Number of samples
Fig. 1B	S2C-DNA-PAINT	MP	60k	50	50	0.71	1.7	70	662	1 image 70 datapoints/ch
Fig. 1B	S2C-DNA-PAINT	MP	40-60k	50-100	50-67	0.80	1.7	70	662	2 images 70 datapoints/ch
Fig. 1C	S2C-DNA-PAINT	MP	25-60k	30	13-30	0.5-1.0	0.5-0.9	60-80	662	10
Fig. 1C	S2C-DNA-PAINT	MP	25-60k	30	13	0.5-1.0	0.5-0.9	60-80	662	5
Fig. 1C	S2C-DNA-PAINT	MP	25-60k	30	13	0.5-1.0	0.5-0.9	60-80	662	5
Fig. 1 A,D	S2C-DNA-PAINT	MP	40-60k	15-60	10-60	1.1	1.3	50	662	4
Fig. 2B	SD-DNA-PAINT	PBS 10 mM $MgCl_2$	60k	100	37-42		2.5	70	700	2 images 39-46 datapoints/ch
Fig. 2C	SD-dSTORM	ABL 50 mM MEA	15-60k	2.6-25	3-9		1.2-13.6	30-100	700	7
Fig. 2C	SD-dSTORM	ABL 50 mM MEA	15-60k	2.6-50	3-13		1.2-13.6	30-100	700	4
Fig. 2 A,D	SD-dSTORM	ABL 100 mM MEA	30-50k	2.6-5	3-5		13.6-30.6	20-30	700	5
Fig. 3	S2C-DNA-PAINT	MP	45k	30	22.5	1.0	0.5	60	662	1-2/condition total=10
Fig. 4	SD-dSTORM	ABL 100 mM MEA	50-60k	15	12.5-15		4.9-6.0	45-50	700	7-9/condition total=48
Fig. 5 A,B,C	S2C-DNA-PAINT	MP	60k	100	100	0.4	0.4	75	662	1
Fig. 5 D,E,F	SD-dSTORM	ABL 100 mM MEA	60k	10	10		6.0	45	700	1
Fig. 6 A,C,F	SD-dSTORM	ABL 50 mM MEA	15-60k	2.6-25	3-9		1.2-13.6	30-100	700	7
Fig. 6 A,C,F	SD-dSTORM	ABL 50 mM MEA	15k	12.5-25	3-7		1.9-3.4	60-80	700	3
Fig. 6 A,C,F	SD-dSTORM	ABL 50 mM MEA	15-60k	2.6-50	3-13		1.2-13.6	30-100	700	4
Fig. 6D	SD-dSTORM	ABL 100 mM MEA	60k	50	25-36		1.5-1.9	80-90	700	3
Fig.S2B	S2C-dSTORM	ABL 100 mM MEA	50k	10	9	3.4	4.9	50	662	1
Fig.S2A	S2C-dSTORM	ABL 100 mM MEA	40k	15	10	2.4	3.4	60	662	1
Fig.S2A	S2C-dSTORM	ABL 100 mM MEA	30k	50	25	1.7	2.5	70	662	1

* Buffer MP: Massive Photonics, ABL: ABBELIGHT

Table S2: Statistical tests (related to Figure 3)

Experiment	*First condition*	*Second condition*	*Third condition*	*N*	*p-value*	*ns: non significant *: p<0.05*
β2-spectrin-F1-Cy3B constant	100% β2-spectrin-F1-Cy3B	100% β2-spectrin-F1-Cy3B		16	0,900	ns
	100% β2-spectrin-F1-Cy3B		100% β2-spectrin-F1-Cy3B	16	0,900	ns
		100% β2-spectrin-F1-Cy3B	100% β2-spectrin-F1-Cy3B	11	0,900	ns
adducin-F2-Atto643 varying	3% Adducin-F2-Atto643	10% Adducin-F2-Atto643		16	0,001	*
	3% Adducin-F2-Atto643		100% Adducin-F2-Atto643	16	0,001	*
		10% Adducin-F2-Atto643	100% Adducin-F2-Atto643	11	0,900	ns
β2-spectrin-F1-Cy3B varying	3% β2-spectrin-F1-Cy3B	10% β2-spectrin-F1-Cy3B		22	0,001	*
	3% β2-spectrin-F1-Cy3B		100% β2-spectrin-F1-Cy3B	12	0,001	*
		10% β2-spectrin-F1-Cy3B	100% β2-spectrin-F1-Cy3B	10	0,900	ns
adducin-F2-Atto643 constant	100% Adducin-F2-Atto643	100% Adducin-F2-Atto643		22	0,001	*
	100% Adducin-F2-Atto643		100% Adducin-F2-Atto643	12	0,001	*
		100% Adducin-F2-Atto643	100% Adducin-F2-Atto643	10	0,230	ns

Table S3: Statistical tests (related to Figure 4)

Experiment	*First condition*	*Second condition*	*Third condition*	*N*	*p-value*	*ns: non significant *: p<0.05*
adducin-AF647 constant	100% adducin-AF647	100% adducin-AF647		50	0,001	*
	100% adducin-AF647		100% adducin-AF647	50	0,105	ns
		100% adducin-AF647	100% adducin-AF647	81	0,062	ns
β2-spectrin-CF680 varying	3% β2-spectrin-CF680	10% β2-spectrin-CF680		50	0,001	*
	3% β2-spectrin-CF680		100% β2-spectrin-CF680	50	0,001	*
		10% β2-spectrin-CF680	100% β2-spectrin-CF680	81	0,445	ns
adducin-AF647 varying	3% adducin-AF647	10% adducin-AF647		60	0,900	ns
	3% adducin-AF647		100% adducin-AF647	59	0,001	*
		10% adducin-AF647	100% adducin-AF647	81	0,001	*
β2-spectrin-CF680 constant	100% β2-spectrin-CF680	100% β2-spectrin-CF680		60	0,900	ns
	100% β2-spectrin-CF680		100% β2-spectrin-CF680	59	0,900	ns
		100% β2-spectrin-CF680	100% β2-spectrin-CF680	81	0,900	ns